Modulation of innate immune signaling by a Coxiella burnetii eukaryotic-like effector protein

Melanie Burette, Julie Allombert, Karine Lambou, Ghizlane Maarifi, Sébastien Nisole, Elizabeth Di Russo Case, Fabien P. Blanchet, Cedric Hassen-Khodja, Stéphanie Cabantous, James Samuel, et al.

Modulation of innate immune signalling by a *Coxiella burnetii* eukaryotic-like effector protein

Melanie Burette[*1], *Julie Allombert*[*1], *Karine Lambou*[1], *Ghizlane Maarifi*[1], *Sebastien Nisole*[1], *Elizabeth Di Russo Case*[2], *Fabien Blanchet*[1], *Cedric Hassen-Khodja*[3], *Stephanie Cabantous*[4], *James E. Samuel*[2], *Eric Martinez*[1], *Matteo Bonazzi*[1]

1. IRIM, CNRS, Université de Montpellier, Montpellier, France.
2. Department of Microbial and Molecular Pathogenesis, Texas A&M Health Science Center College of Medicine, Bryan, Texas 77807–3260, USA
3. MRI, BioCampus Montpellier, CNRS, INSERM, Université de Montpellier, Montpellier, France.
4. Centre de Recherche en Cancérologie de Toulouse (CRCT), Inserm, Université Paul Sabatier-Toulouse III, CNRS, Toulouse, France

* These authors contributed equally to this work

For correspondence: matteo.bonazzi@irim.cnrs.fr

Abstract

The Q fever agent *Coxiella burnetii* uses a defect in organelle trafficking/intracellular multiplication (Dot/Icm) Type 4b Secretion System (T4SS) to silence the host innate immune response during infection. By investigating *C. burnetii* effector proteins containing eukaryotic-like domains, here we identify NopA (for Nucleolar protein A), which displays 4 Regulator of Chromosome Condensation (RCC) repeats, homologous to those found in the eukaryotic Ras-related nuclear protein (Ran) guanine nucleotide exchange factor (GEF) RCC1. Accordingly, NopA is found associated with the chromatin nuclear fraction of cells and uses the RCC-like domain to interact with Ran. Interestingly, NopA triggers an accumulation of Ran-GTP, which accumulates at nucleoli of transfected or infected cells, thus perturbing the nuclear import of transcription factors of the innate immune signalling pathway. Accordingly, qRT-PCR analysis on a panel of cytokines shows that cells exposed to the *C. burnetii nopA*::Tn or a Dot/Icm-defective *dotA*::Tn mutant strains present a functional innate immune response, as opposed to cells exposed to wt *C. burnetii* or the corresponding *nopA* complemented strain. Thus, NopA is an important regulator of the innate immune response allowing *Coxiella* to behave as a stealth pathogen.

Significance statement

Coxiella burnetii is a stealth pathogen that evades innate immune recognition by inhibiting the NF-κB signalling pathway. This process is mediated by the bacterial Dot/Icm secretion system; however, the bacterial effector/s, as well as the molecular mechanism involved in this process remained to date unknown. Here, by investigating *C. burnetii* proteins with eukaryotic-like features (EUGENs), we discovered a new effector protein, NopA (for Nucleolar protein A), which localizes at nucleoli of infected cells and perturbs nucleocytoplasmic transport by manipulating the intracellular gradients of the GTPase Ran. In doing so, NopA reduces the nuclear levels of transcription factors involved in the innate immune sensing of pathogens and single-handedly downmodulates the expression of a panel of cytokines.

Introduction

The nuclear factor kappa-light-chain-enhancer of activated B cells (NF-κB) family of transcription factors regulates the expression of genes associated with diverse cellular functions and plays a central role in regulating the innate and acquired host immune response to bacterial infections (1, 2). Under physiological conditions, the transcription factors of the NF-κB family are sequestered in the cytoplasm by specific interactions with nuclear factor kappa-light polypeptide gene enhancer in B cells inhibitor alpha (IκBα), which mask the nuclear localisation signal (NLS) on transcription factors. Exogenous signals, including recognition of the tumour necrosis factor (TNF) by TNF receptor or the bacterial lipopolysaccharide (LPS) by Toll-like Receptor 4 (TLR4), activate the NF-κB signalling pathway by triggering the phosphorylation and proteasomal degradation of IκBα, thus unmasking the NLS on transcription factors. The signal is then recognised by importin-α and members of the importin-β family, which mediate the translocation of transcription factors to the nucleus through nuclear pore complexes (1). Energy for nuclear transport of NLS-containing proteins is provided by intracellular gradients of the small GTPase Ras-related nuclear protein (Ran), which interacts with the importin complexes upon nuclear import. GDP-bound Ran is largely cytoplasmic and nuclear translocation triggers the conversion to the GTP-bound form by means of the Ran guanine nucleotide exchange factor (GEF) RCC-1 (regulator of chromosome condensation-1). In its GTP-bound form, Ran triggers the dissociation of importins from the cargo and importin complexes recycle back to the cytoplasm. There, Ran GTPase activating protein (RanGAP) generates Ran-GDP, which dissociates from importin complexes (3).

Given its pivotal role in the antimicrobial response, it is not surprising to observe that a considerable number of bacterial pathogens deploy effector proteins that modulate the NF-κB

signalling pathway (1, 2). These are mostly involved in phosphorylation, ubiquitination and proteasomal degradation of components of the NF-κB complex, whereas other modulate NF-κB-mediated transcription (1, 2). Interestingly, it has been recently reported that *Salmonella* and *Orientia tsutsugamushi* effector proteins can interfere with nucleocytoplasmic transport, thereby inhibiting nuclear translocation of the p65/RelA transcription factor (4, 5).

The Q fever pathogen *Coxiella burnetii* is an obligate intracellular bacterium that relies on the translocation of effector proteins by a defect in organelle trafficking/intracellular multiplication (Dot/Icm) Type 4b Secretion System (T4SS) to replicate within large autolysosomal-like compartments inside infected cells (6, 7). Bioinformatics analysis identified over 140 *C. burnetii* genes encoding candidate effector proteins (7); however, the majority of these remain under-investigated due to the technical constraints associated with the genetic manipulation of this organism. A subset of effector proteins is involved in the biogenesis of *Coxiella*-containing vacuoles (CCVs), by rerouting membrane traffic to the bacterial replicative niche, while other effectors manipulate the apoptotic and inflammatory pathways to ensure intracellular persistence (6). Importantly, *C. burnetii* behaves as a stealth pathogen, evading the host innate immune response by down-modulating the NF-κB and the inflammasome signalling pathways (8, 9). The *C. burnetii* effector protein IcaA (Inhibition of caspase activation A) inhibits NOD-like receptor family pyrin domain containing 3 (NLRP3)-mediated inflammasome activation induced by caspase-11 (8), whereas the NF-κB signalling pathway is down-modulated in a Dot/Icm-dependent manner, by perturbing the nuclear translocation of the p65/RelA subunit, without affecting the overall cellular levels of p65 (9). However, the bacterial effector/s involved in this process remain uncharacterised (9). We have previously reported the large-scale phenotypic characterisation of *C. burnetii* transposon mutants library, which allowed to gain important insights into the function of the Dot/Icm secretion system, and highlight an important

set of virulence determinants (10–12). Importantly, several genes involved in intracellular replication of *C. burnetii* encode proteins with predicted eukaryotic-like domains, which prompted us to investigate eukaryotic-like genes (EUGENs) on a genome-wide scale. Here, we identify and validate the Dot/Icm-mediated translocation of 7 *C. burnetii* EUGENs. Among these, NopA (for Nucleolar protein A) displays 4 Regulation of Chromosome Condensation (RCC) repeats, which are partially homologous to the 7 repeats found in the bladed β-propeller structure of the Ran GEF RCC1 (13–15). Similar to RCC1, NopA also localises at the nucleus of infected or transfected cells, it is found associated with the chromatin nuclear fraction, and uses the RCC-like domain to interact with Ran. Differently from RCC1 however, NopA accumulates at nucleoli and sequesters Ran, thus perturbing nucleocytoplasmic transport. Indeed, NopA perturbs nuclear translocation of p65 upon cell treatment with TNF-α or challenge with *C. burnetii*. Conversely, transposon insertions in the *nopA* gene restore nuclear translocation of p65 during infections, to levels that are similar to those observed with the Dot/Icm-deficient *C. burnetii dotA* mutant. Accordingly, myeloid cells challenged with the *C. burnetii nopA* or *dotA* mutant strains present a functional innate immune response, as opposed to myeloid cells exposed to wt *C. burnetii* or the *nopA* complemented strain.

Results

Identification of *C. burnetii* EUGENS

The Searching Algorithm for Type IV Effector proteins (S4TE) 2.0 (16) was used to identify *C. burnetii* eukaryotic-like genes (EUGENs) encoding candidate effector proteins. This allowed the identification of 56 genes, which were validated using the PFAM, SMART, CDD and ELM databases (Table S1). Of these, 20 candidate EUGENS were retained for further analysis (Table S2), based on the S4TE score (16), the eukaryotic-like domain encoded and the presence of corresponding transposon mutants in our library (10). *cbu0072* (*ankA*), *cbu0201* (*ankC*), *cbu0447* (*ankF*), *cbu0781* (*ankG*) and *cbu1213* (*ankI*) encode Ankyrin repeats (17, 18); *cbu0295, cbu0547* and *cbu1457* (*cig43*) encode tetratricopeptide repeats; *cbu0175* and *cbu1379a* encode predicted Ser/Thr kinases; *cbu0801* (*rimI*), *cbu0505* (*cig14*) and *cbu1799* encode acetyltransferases; *cbu0096* encode a predicted phospholipase D; *cbu0519* (*dedA*) encodes a SNARE-like domain-containing protein; *cbu1206* encodes a predicted sterol reductase; *cbu1217* encodes a protein with 4 Regulation of Chromosome Condensation (RCC) repeats; *cbu1724* encodes a predicted F-box protein; *cbu1366* (*cig40*) encodes a coiled-coil domain-containing protein and *cbu0542* (*ligA*) encodes a predicted DNA-ligase (Table S2). Of note, Dot/Icm-dependent translocation of proteins encoded by 8 of these genes has been previously validated using *L. pneumophila* as a surrogate system (17, 19, 20) (Table S2). Selected genes were cloned into pXDC61K-*blaM* vector, thus generating N-terminal fusions with β-lactamase, and transformed into *C. burnetii* NMII RSA439. The expression of 16 out of 20 chimeric proteins was validated by Western blot using an anti-β-lactamase antibody (Fig. S1A). Candidate effector protein translocation was assessed at 6, 12, 24, 48, and 72 hours post-infection using the β-lactamase assay. *C. burnetii* expressing β-lactamase alone or β-lactamase-tagged CvpB (CBU0021) (12) were used as negative and positive controls, respectively. CvpB, CBU0295, and

CBU1217 were efficiently translocated from 12 hours post-infection, whereas AnkA, F and G were translocated from 24 hours post-infection (Fig. 1A, B). Finally, AnkC, CBU0175 and CBU1724 were also translocated, albeit less efficiently, at later time points of infection (Fig. 1A, B). Plasmids encoding translocated effectors were then transformed into the *C. burnetii dotA*::Tn strain to validate their Dot/Icm-dependent secretion at 72 hours post-infection. The expression of 6 chimeric proteins was validated by Western blot using an anti-β-lactamase antibody (Fig. S1B). None of the effector proteins were secreted by the Dot/Icm-defective mutant as expected (Fig. 1A). Next, *cbu0072* (*ankA*), *cbu0295*, *cbu0447* (*ankF*), *cbu0781* (*ankG*) and *cbu1217* were cloned into a pLVX-mCherry vector to tag effector proteins at their N-terminal domain and investigate their localisation in non-infected and *C. burnetii*-infected U2OS cells (Fig. 1C). AnkA and CBU0295 were mostly diffuse in the cytoplasm and did not localise at CCVs in infected cells. AnkF displayed a punctate pattern in the cytoplasm, which partially colocalised with the lysosomal marker LAMP1 in non-infected and infected cells alike (Fig. 1C). Differently from previous reports, indicating a translocation of AnkG from mitochondria to the nucleus of transfected cells following staurosporine treatment (21), in our hands, this effector protein displayed nuclear localisation even in the absence of staurosporine, in both infected and non-infected cells (Fig. 1C). Of note, CBU1217 was exclusively localised at sub-nuclear structures in over 90% of either infected or non-infected cells (Fig. 1C).

The effector protein CBU1217 localises at nucleoli in infected and transfected cells

The localisation of CBU1217 was further investigated by cloning the gene into a pJA-LacO-4HA plasmid, to express the effector protein carrying an N-terminal 4xHA tag in *C. burnetii*, under the control of an IPTG promoter, and monitor its localisation during infection. GFP-expressing wt *C. burnetii* or the *dot/icm* mutant *dotA*::Tn (10) were transformed either with

pJA-LacO-4HA or with pJA-LacO-4HA-*cbu1217*. Expression of 4HA-CBU1217 was validated by Western blot using an anti-HA antibody (Fig. S1C). U2OS cells were challenged with the transformed *C. burnetii* strains and NopA localisation was assessed, in the presence or absence of IPTG, using anti-HA and anti-fibrillarin antibodies and Hoechst dye. Infections by *C. burnetii* transformed with pJA-LacO-4HA-*cbu1217* in the absence of IPTG did not show specific HA labelling (Fig. 2A). Addition of 1mM IPTG triggered 4HA-CBU1217 expression, which co-localised with fibrillarin in over 90% of HA-positive cells (Fig. 2B). The intracellular localisation of 4HA-CBU1217 was lost when cells were infected with the *dotA*::Tn mutant transformed with pJA-LacO-4HA-*cbu1217* in the presence of IPTG (Fig. 2D), confirming that CBU1217 is a Dot/Icm substrate. Induction of the expression of the HA tag alone did not show specific localisation (Fig. 2C). We thus named the new *C. burnetii* EUGEN NopA, for Nucleolar protein A.

As mentioned above, NopA encodes 4 RCC repeats in its C-terminal domain (Fig. 2E). In the eukaryotic protein RCC1, 7 repeats are arranged in a 7-bladed propeller, which associates with nuclear chromatin and acts as a GEF for Ran, thus regulating nucleocytoplasmic protein transport (3). To determine the role of the RCC-like domain in NopA localisation and function, the effector protein was cloned into a pRK5-HA plasmid to generate HA-tagged NopA. U2OS cells transfected with pRK5-HA-NopA were processed for immunofluorescence using Hoechst dye, anti-HA and anti-fibrillarin antibodies. In parallel, HA-NopA localisation was investigated by Western blot using U2OS cells transfected as above, lysed and separated into cytoplasmic, nuclear and chromatin fractions. Full length NopA ($NopA_{FL}$) localised at nucleoli in over 90% of transfected cells, confirming our observations in the context of *C. burnetii* infections (Fig. 2E). Western blot analysis confirmed that NopA is excluded from the cytoplasmic fraction and localised at the soluble and chromatin nuclear fractions (Fig. 2E). Next, we generated HA-tagged

NopA deletions to exclude ($NopA_{N\text{-}ter}$; aa 1-195, Fig. 2F) or include ($NopA_{C\text{-}ter}$; aa 196-497, Fig. 2G) the RCC repeats. Ectopically expressed HA-$NopA_{N\text{-}ter}$ was excluded from nuclei and remained diffuse in the cytoplasm (Fig. 2F) whereas HA-$NopA_{C\text{-}ter}$ retained the nucleolar localisation (Fig. 2G). Cell fractionation confirmed the cytoplasmic localisation of HA-$NopA_{N\text{-}ter}$ and the nuclear localisation of HA-$NopA_{C\text{-}ter}$, as well as the association with the chromatin fraction (Fig. 2F, G). Thus, despite the lack of typical nuclear or nucleolar localisation signals, the C-terminal domain of NopA encoding the RCC-like domain, is necessary and sufficient for the nucleolar targeting of the effector protein. The role of the RCC repeats in the intracellular localisation of NopA was further dissected by generating increasing deletions of single RCC repeats (numbered from 1 to 4 from the N-terminal) from either the N-terminal or C-terminal ends of HA-$NopA_{C\text{-}ter}$ (Fig. S2A). The intracellular localisation of each construct was tested by immunofluorescence and cell fractionation following ectopic expression in U2OS cells. Interestingly, this revealed that the first RCC repeat is critical for targeting NopA to the nucleus as removal of this repeat from $NopA_{C\text{-}ter}$ displaces the protein to the cytoplasm (Fig. S2B, C). The first 2 RCC repeats (RCC12; aa 196-310) alone localise within the nucleus but are excluded from nucleoli (Fig. S2E) and instead localise at promyelocytic leukaemia (PML) bodies (Fig. S2G). This localisation remains unchanged with the addition of the 3rd RCC repeat (Fig. S2D, F), and it is only with the addition of the complete $NopA_{C\text{-}ter}$ that the protein localises at nucleoli (Fig. 2G), suggesting the presence of a nucleolar-targeting motif in the 4th RCC repeat. Unfortunately, we were unable to express detectable amounts of single RCC repeats (RCC1 and RCC4, Fig. S2A).

NopA is not involved in *C. burnetii* intracellular replication

Given the early translocation of NopA observed using the β-lactamase assay, we determined the time course of NopA production during infection. To this aim, we have

complemented the *nopA* mutation, using a mini Tn7 transposon to integrate a wild type copy of HA-tagged *nopA*, under the regulation of its predicted endogenous promoter, in the chromosome of the *C. burnetii Tn227* strain, which carries the transposon insertion closest to the *nopA* start codon (10). Protein expression was then monitored by Western blot, using an anti-HA antibody, from cells challenged with the complemented *nopA*::Tn strain for 12, 24, 48, and 72 hours. By this approach, detectable amounts of NopA were observed from 12 hours post-infection (Fig. S1D).

We previously reported that transposon insertions in *nopA* do not affect bacterial replication in Vero cells (10). To further investigate the role of NopA in *C. burnetii* infections, bacterial replication and virulence of the wild type, *dotA*::Tn, *nopA*::Tn, and the *nopA*::Tn complemented strain (*nopA*::Tn Comp.) described above, were tested using either bone marrow-derived macrophages (BMDM) or a SCID mouse model of infection. Confirming our initial observations, transposon insertions in *nopA* do not affect *C. burnetii* replication (Fig. 2H, I) or virulence (as determined here by splenomegaly measurements, Fig. 2J).

NopA interacts with the small GTPase Ran

Given that NopA localises at nucleoli and presents 4 out of the 7 RCC repeats present in the eukaryotic Ran-GEF RCC1, we investigated whether NopA can interact with Ran. To this aim, U2OS cells incubated either with the *nopA*::Tn mutant or the complemented strain expressing 4HA-tagged NopA under the control of the predicted endogenous promoter (*nopA*::Tn Comp.). Twenty-four hours post-infection, cells were lysed, separated into cytoplasmic, nuclear and chromatin fractions, and NopA was immuno-captured from cell fractions using an anti-HA antibody. As expected, NopA was not detected in cells infected with the *nopA*::Tn mutant strain, whereas it was efficiently isolated from the nuclear and chromatin fractions of cells challenged

with the complemented strain (Fig. 3A). Of note, whole cell lysates of cells incubated with the complemented strain also presented an accumulation of Ran in the chromatin fraction, which was not observed in cells challenged with the *nopA*::Tn mutant strain (Fig. 3A). Importantly, Ran was efficiently detected, together with NopA, in immunoprecipitates from the nuclear and chromatin fractions of cells challenged with the *nopA*::Tn complemented strain, indicating indeed an interaction with the *C. burnetii* effector protein (Fig. 3A). The NopA/Ran interaction was further investigated in U2OS cells, following the ectopic expression of either HA-tagged $NopA_{N\text{-}ter}$, $NopA_{C\text{-}ter}$ or the *C. burnetii* effector protein CvpF as negative control (22). Unfortunately, under these conditions, we were unable to immuno-precipitate full-length NopA from transfected cells. Similarly to infected cells, 24 hours post-transfection, cells were lysed, separated into cytoplasmic, nuclear and chromatin fractions, and NopA truncations and CvpF were immuno-captured from cell fractions using an anti-HA antibody. As expected, $NopA_{N\text{-}ter}$ and CvpF were efficiently isolated from the cytoplasmic fractions, whereas $NopA_{C\text{-}ter}$ was isolated from the nuclear and cytoplasmic fractions (Fig. 3B). In agreement with what we observed in infected cells, the ectopic expression of $NopA_{C\text{-}ter}$ triggered an accumulation of Ran to the chromatin fractions (Fig. 3B). Moreover, Ran was specifically detected in the nuclear and chromatin fractions upon immune-capturing of $NopA_{C\text{-}ter}$, confirming an interaction between the two proteins (Fig. 3B). Of note, no interaction was detected between Ran and $NopA_{N\text{-}ter}$, despite their shared cytoplasmic localisation (Fig. 3B). Furthermore, $NopA_{C\text{-}ter}$ did not interact with other small GTPases such as DRP1 or RAB26, nor with the nucleolar marker fibrillarin (Fig. 3B). Conversely, the *C. burnetii* effector protein CvpF (22), was readily immuno-captured from the cytoplasm of transfected cells and interacted with RAB26 as reported (22) (Fig. 3B).

Finally, the direct interaction between NopA and Ran was further investigated using the tripartite split-GFP interaction sensor (23). Briefly, the assay is based on a tripartite association

between two GFP β-strands (GFP10 and GFP11), fused to proteins of interest, and the complementary GFP1-9 detector. If proteins interact, GFP10 and GFP11 self-associate with GFP1-9 to reconstitute a functional GFP. pCDNA3-zipper-GFP10 and pCDNA3-zipper-GFP11 were used as negative control, whereas a plasmid encoding GFP10 and GFP11 linked by a zipper motif (GFP10-zip-GFP11) was used as positive control (23). *ran* cDNA was cloned into the pCDNA3-GFP10-zipper plasmid to generate the GFP10-Ran, whereas *nopA*, *rcc1* and *fbl* (the gene encoding fibrillarin) were cloned into the pCDNA3-zipper-GFP11 plasmid to generate the corresponding GFP11 fusion proteins. Combinations of the above-mentioned constructs with a pCMV plasmid encoding GFP1-9 were used for triple transfections in U2OS cells. After fixation, an anti-GFP antibody was used to identify cells expressing GFP1-9 (which is not fluorescent) and protein interactions were analysed by monitoring GFP reconstitution. As expected, co-expression of GFP1-9 with GFP10 and GFP11 did not result in the reconstitution of GFP (Fig. 3C, top row, and 3D). The co-expression of GFP1-9 with GFP10-zip-GFP11 led to the reconstitution of GFP fluorescence in over 93% of transfected cells, demonstrating the functionality of the assay (Fig. 3C, centre row, and 3D). Importantly, over 60% of cells expression GFP1-9 in combination with GFP10-Ran and GFP11-NopA showed reconstitution of GFP, with a fluorescent signal detected at nuclei, with a strong accumulation at nucleoli (Fig. 3C, bottom row, and 3D). On the contrary, the expression GFP1-9 in combination with GFP10-Ran and GFP11-RCC1, which allowed reconstitution of GFP fluorescence homogeneously detected in the nucleus in over 73% of transfected cells (Fig. S3A, and 3D). Lack of GFP reconstitution upon expression of GFP1-9 in combination with GFP10-Ran and GFP11-fibrillarin indicated that the shared nucleolar localisation was not sufficient for GFP reconstitution (Fig. S3A, and 3D).

Ectopic expression of either mCherry-NopA$_{FL}$ or mCherry-NopA$_{C\text{-}ter}$ in combination with GFP-Ran in U2OS cells also confirmed the co-localisation of both proteins at nucleolar structures labelled with the anti-fibrillarin antibody (Fig. S3B), Conversely, Ran-GFP accumulation at nucleoli was lost when the small GTPase was ectopically expressed in U2OS cells in combination either with mCherry alone or mCherry-NopA$_{N\text{-}ter}$ (Fig. S3B). Collectively, these observations indicate that NopA specifically interacts with Ran and may sequester it at nucleoli.

NopA preferentially interacts with GDP-bound Ran and triggers an increase in Ran-GTP

To determine whether NopA displays preferential binding to Ran in its GDP- versus GTP-bound form, a GFP-trap assay was carried out on U2OS cells co-transfected with plasmids encoding HA-NopA$_{C\text{-}ter}$ in combination with either GFP alone, GFP-Ran, GFP-Ran$_{T24N}$ (GDP-locked), GFP-Ran$_{Q69L}$ (GTP-locked) or GFP-Ran$_{N122I}$ (nucleotide-free form). Similar to RCC1, NopA displayed preferential binding to either GDP-locked Ran$_{T24N}$ or the nucleotide-free form Ran$_{N122I}$ (Fig. 4A).

Next, we investigated whether NopA binding to Ran can affect the Ran GDP/GTP ratio that is required to fuel nucleocytoplasmic transport. U2OS cells were challenged either with wt *C. burnetii*, the *dotA*::Tn, *nopA*::Tn, or the *nopA*::Tn complemented strains. Non-infected cells were used as control. Twenty-four hours post-infection, cells were lysed and incubated with agarose beads coated with the Ran effector Ran-Binding Protein 1 (RanBP1), to specifically pull-down the GTP-bound form of Ran. Indeed, infection with wt *C. burnetii* triggered a 40-fold increase in the intracellular levels of Ran-GTP, as compared to non-infected cells (Fig. 4B). This phenotype was lost in cells challenged with the *dotA*::Tn mutant strain and only an 8.5-fold increase was observed in cells challenged with the *nopA*::Tn mutant strain. Increased levels of Ran-GTP were largely restored (35-fold increase) in cells exposed to the complemented strain

(*nopA*::Tn Comp., Fig. 4B). The effects of NopA on the intracellular levels of Ran-GTP were further investigated in U2OS cells transfected with plasmids encoding either HA alone, HA-NopA, HA-NopA$_{N\text{-}ter}$, HA-NopA$_{C\text{-}ter}$, or the *C. burnetii* effector protein CvpB (12) used here as negative control. A three-fold increase in the intracellular levels of Ran-GTP was observed in cells expressing either HA-NopA or HA-NopA$_{C\text{-}ter}$, as compared to cells transfected with HA alone or HA-NopA$_{N\text{-}ter}$ (Fig. 4C). As expected, ectopic expression of CvpB had negligible impact on the intracellular levels of Ran-GTP (Fig. 4C). These observations suggest that NopA sequestration of Ran at nucleoli leads to an increase in the intracellular levels of Ran-GTP, which may negatively regulate nuclear import (24).

NopA perturbs protein translocation to the nucleus

Given the role of Ran in nucleocytoplasmic traffic, and the previously reported observation that *C. burnetii* infections modulate nuclear translocation of p65 by a Dot/Icm-dependent mechanism (9), we investigated whether NopA affects the nuclear localisation of p65, which follows the activation of the NF-κB signalling pathway. U2OS cells transfected with plasmids encoding either HA- or mCherry-tagged versions of NopA were either left untreated or challenged with 10 ng/ml TNF-α for 30 minutes, and the nuclear translocation of p65 was monitored using an anti-p65 antibody either by fluorescence microscopy or Western blot following cell fractionation. Cells expressing either HA- or mCherry-tagged CvpB or the tags alone were used as controls. TNF-α treatment efficiently activated the NF-κB pathway, as indicated by the significant degradation of IκBα (Fig. 5A). Accordingly, p65 was readily re-localised to the nucleus of cells expressing either the HA or mCherry tags alone or tagged versions of the *C. burnetii* effector CvpB (Fig. 5B, C and D). However, p65 translocation was

largely inhibited in cells expressing either HA-NopA or mCherry-NopA (Fig. 5B, C and D). In all cases, the intracellular levels of p65 remained largely unaltered. To determine whether NopA modulates the intracellular levels of p65 by perturbing its nuclear import or by accelerating its nuclear export, U2OS cells expressing either mCherry-NopA, mCherry-CvpB or mCherry alone as controls, were incubated for 4 hours with 5 nM leptomycin B (LMB), a fungal metabolite that blocks nuclear export by covalently binding to exportin 1. As p65 shuttles continuously between the nucleus and the cytoplasm, treatment with LMB in mCherry- or mCherry-CvpB expressing cells led to an accumulation of the transcription factor in the nucleus (Fig. 5D, S4). Interestingly however, ectopic expression of mCherry-NopA significantly prevented p65 nuclear accumulation in response to LMB treatment (Fig. 5D, S4). A similar phenotype was observed in cells treated with LMB for 4 hours, followed by 30 min incubation with TNF-α (Fig. 5D, S4). These data indicate that indeed, NopA perturbs nuclear import.

Next, we tested whether the perturbation of nuclear import triggered by NopA was specific to p65 and *C. burnetii* infections. The nuclear translocation of the transcription factor IRF3 was monitored in U2OS cells co-transfected with 3FLAG-tagged IRF3 in combination with either mCherry alone, mCherry-NopA or mCherry-CvpB, and infected with the Sendai Virus for 18 hours. Non-infected cells were used as control (Fig. S5A). Similar to what we reported for p65, IRF3 was readily translocated to the nuclei of cells expressing either mCherry alone or mCherry-CvpB but remained largely cytoplasmic in cells expressing mCherry-NopA (Fig. S5A, B).

NopA is involved in the silencing of the innate immune response during *C. burnetii* infections

p65 nuclear translocation was further monitored in U2OS cells non-infected or challenged either with 10 ng/ml TNF-α for 30 minutes, wt *C. burnetii*, the Dot/Icm-defective mutant *dotA*::Tn, the *nopA*::Tn or the complemented strain (*nopA*::Tn Comp.), for 24, 48 and 72 hours by fluorescence microscopy and, for the 72 hours time point, by Western blot following cell fractionation. IκBα was significantly degraded in all conditions as compared to non-infected cells, indicating an efficient activation of the NF-κB pathway (Fig. 6A). Translocation of p65 to the nucleus was readily detected in cells treated with TNF-α, either by Western blotting (Fig. 6B) or by immunofluorescence (Fig. 6C, D). Cells challenged with wt *C. burnetii* or the *nopA*::Tn complemented strain showed a small but significant increase in nuclear p65 fluorescence as compared to non-infected, untreated cells (Fig. 6B, C, D). However, incubation with either the *dotA*::Tn or the *nopA*::Tn mutants triggered an accumulation of p65 to the nucleus which was comparable to the TNF-α treatment (Fig. 6B, C, D). Measurement of p65 nuclear translocation by immunofluorescence, which was specifically measured in infected cells, resulted in a stronger phenotype as compared to Western blot analysis, which was carried out on the total cell population.

To investigate the downstream effects of perturbing the nuclear translocation of transcription factors involved in the immune response to *C. burnetii* infections, differentiated THP-1 macrophages were exposed to either wt *C. burnetii*, the Dot/Icm-deficient *dotA*::Tn mutant, the *nopA*::Tn mutant or the corresponding complemented strain (*nopA*::Tn Comp.) for 24, 48 and 72 hours. Total RNA was extracted from cell lysates and qRT-PCR analysis was used to monitor the expression of a panel of cytokines (Fig. 7A, S6A). A slight increase in the mRNA expression levels of all tested cytokines was observed in cells exposed to wt *C. burnetii* or the *nopA*::Tn complemented strain, as compared to non-infected cells. Interestingly however, cells

exposed to either the *dotA*::Tn mutant or the *nopA*::Tn mutant displayed a comparable, significant increase in the production of the majority of the cytokines tested, ranging from a two-fold increase to a 100-fold increase for IL8 (Fig. 7A, S6A, S7). Downmodulation of the innate immune response was further confirmed by monitoring TNF-α and IFN-α production in THP-1 macrophages infected as above for 72 and 96 hours. As *C. burnetii* effectors are known to perturb the secretory pathway of infected cells (20, 25), THP-1 cells were treated with brefeldin A (BFA) 24 hours prior to fixation and the intracellular levels of TNF-α and IFN-α were assessed by flow cytometry (Fig. 7B, C), following the application of a specific gating to isolate the population of infected cells (Fig. S6B). A significant increase in the intracellular levels of both cytokines was observed in cells infected either with the *nopA*::Tn or the *dotA*::Tn strains as compared to cells infected with wt *C. burnetii* or the *nopA*::Tn complemented strain (Fig. 7B, C). Overall, our data indicate that *C. burnetii* uses the Dot/Icm secretion system to down-modulate the NF-κB signalling pathway as previously reported (9), and that NopA is a key effector for this process.

Discussion

Intracellular bacterial pathogens and symbionts establish intimate interactions with their eukaryotic hosts, which have evolved by co-evolution over time. Part of their adaptation to their intracellular niches has been mediated by trans-kingdom acquisition and functional integration of eukaryotic genes in bacterial genomes (26). Indeed, Eukaryotic-like GENes (or EUGENs), represent a hallmark of intracellular bacteria, and are rarely observed in free-living bacteria. Importantly, many EUGENs from intracellular bacteria produce candidate or validated effector proteins that are translocated into host cells through dedicated type III or type IV secretion systems (27). Thus, EUGENs are predicted to play an important role in the establishment of parasitic or symbiotic bacterial lifestyles.

In this study, bioinformatics analysis combined with translocation assays led to the identification of 7 *C. burnetii* effector proteins encoding eukaryotic-like domains involved in protein/protein interactions, protein/chromatin interactions and post-translational modifications. CBU0447 and CBU0175 are conserved among *C. burnetii* strains whereas the remaining 5 EUGENS present some degree of polymorphism (7). Upon ectopic expression in epithelial cells of translocated ankyrin repeats-containing proteins, AnkA (CBU0072) was largely cytoplasmic, whereas AnkF (CBU0447) seemed to associate with membranes that partially co-localised with the lysosomal marker LAMP1. AnkG (CBU0781), which was previously reported to localise at mitochondria and translocate to the nucleus upon staurosporine treatment of transfected cells (21), partially localised to the nucleus even in the absence of staurosporine in our hands. It is thus possible that other Ank proteins modify their intracellular localisation at different stages of infection.

Here, we have focused our study on CBU1217, which encodes 4 RCC repeats in its C-terminal domain (aa 196-497). RCC repeats are found in the Regulation of Chromosome

Condensation 1 (RCC1) eukaryotic protein (28). In eukaryotes, the RCC domain consists of seven homologous repeats of 51-68 amino acid residues, arranged in a β-propeller fold (15). A single RCC domain constitutes the majority of the protein in the case of the RCC1 subgroup of the RCC1 superfamily, whereas multiple RCC domains can be found, either alone or in combination with other functional domains the other subgroups of the superfamily (13). As such, RCCs are versatile domains that can be involved in protein/protein or protein/chromatin interactions, guanine nucleotide exchange factor (GEF) and post-translational modifications including ubiquitination and phosphorylation (13). RCC1 is primarily found in association with histones H2A and H2B on chromatin (29) and acts as a GEF for the small GTPase Ran, a master regulator of nucleocytoplasmic transport during interphase and mitotic spindle assembly during mitosis (30).

Among vacuolar bacterial pathogens, the *L. pneumophila* effector protein LegG1 encodes an RCC-like domain (RLD) consisting of 3 out of the 7 RCC repeats typically found in eukaryotes (31). Of note, LegG1 localises at *Legionella*-containing vacuoles (LCVs) where it recruits and activates Ran to promote microtubule polymerisation and LCV mobility (32). Differently from LegG1, *C. burnetii* NopA encodes an additional RCC repeat and, despite the lack of typical nuclear or nucleolar localisation signals, exclusively localises at nuclei with a strong enrichment in the chromatin fraction, which is consistent with RCC1 localisation. NopA RCC repeats are necessary and sufficient to target the protein to nucleoli and exert its functions. Moreover, the first RCC repeat seems to be critical for targeting NopA to the nucleus as removal of this repeat from $NopA_{C\text{-}term}$ displaces the protein to the cytoplasm. Interestingly, the first 2 RCC repeats (aa 196-310) alone localise at promyelocytic leukaemia (PML) bodies. This localisation remains unchanged with the addition of the 3rd RCC repeat and it is only the

437 expression of the complete $NopA_{C\text{-}term}$ that triggers protein localisation at nucleoli, suggesting the
438 presence of a nucleolar-targeting motif in the 4^{th} RCC repeat.

439 Similarly to the eukaryotic protein RCC1, NopA interacts with Ran, with preferential
440 affinity for the GDP-bound form and promotes the activation of Ran. Differently from RCC1
441 however, NopA also triggers a nucleolar accumulation of Ran. Thus, the observed increase in the
442 intracellular levels of GTP-bound Ran may result from either a GEF activity of NopA (which has
443 been reported for RCC1), or via the observed sequestration of Ran at nucleoli, which would
444 prevent GTP-bound Ran to recycle back to the cytoplasm, where Ran GTPase activating proteins
445 (GAPs) stimulate GTP to GDP conversion. As we were unable to purify sufficient amounts of
446 either full length NopA or $NopA_{C\text{-}ter}$ we could not assess for the moment whether NopA has
447 intrinsic GEF activity. Interestingly, a residual increase in the intracellular levels of Ran-GTP
448 was still observed in cells challenged with the *nopA*::Tn mutant strain, as compared to infections
449 with the Dot/Icm-defective *dotA*::Tn strain. This may suggest that other *C. burnetii* effectors may
450 have a role in the modulation of Ran activity.

451 Of note, mutations in *nopA* do not affect *C. burnetii* intracellular replication (10).
452 However, increasing the intracellular levels of Ran-GTP results in an global alteration in the
453 nucleocytoplasmic transport of proteins (24). It has been reported that during infections,
454 *C. burnetii* requires Dot/Icm activity to downmodulate the NF-κB pathway by perturbing the
455 nuclear translocation of the p65 transcription factor (9). Here we demonstrate that NopA is one of
456 the effector proteins involved in this process, as indicated by the strong inhibition of nuclear
457 translocation of p65 upon treatment of cells with TNF-α or infection. The modulation of the NF-
458 κB signalling pathway has been reported for a number of bacterial pathogen and viruses (1, 2). In
459 most cases, bacteria interfere with the degradation of IκBα and the release of p65 or by

triggering the proteasomal degradation of p65 itself. Other bacteria, including *L. pneumophila* and *Shigella flexneri* may also inhibit the innate immune response downstream of p65 nuclear translocation, at the level of transcription and mRNA processing, respectively (2). Finally, an emerging number of bacterial effectors inhibit NF-κB activation by modulating the nuclear translocation and/or accumulation of p65, by interfering with nucleocytoplasmic protein transport. The *Salmonella* SPI-2 T3SS effector protein SpvD accumulates importin-α in the nucleus by binding exportin Xpo2, thereby preventing p65 nuclear import (4). *O. tsutsugamushi* uses Ankyrin repeats-containing effector proteins Ank1 and 6 by co-opting the function of both importin-β and exportin 1, thus accelerating p65 nuclear export (5). Here we show that the NF-κB pathway is readily activated upon *C. burnetii* infections as shown by efficient IκBα degradation. However, NopA perturbs nuclear accumulation of p65 by triggering the nuclear accumulation of GTP-bound Ran, resulting in an imbalanced Ran gradient across cells. In turn, this leads to a defective nuclear import of proteins, as also demonstrated by challenging cells ectopically expressing NopA with leptomycin B to block nuclear export.

Considering that these bacterial effectors manipulate common adaptors and GTPases involved in nucleocytoplasmic transport, it would be of interest to monitor their effect on a broader panel of proteins and investigate how infected cells respond to these perturbations. For example, other *C. burnetii* effector proteins have been described to localise at the nucleus of infected cells (21, 33, 34). In this perspective, it is important to note that nuclear translocation of p65 is not completely ablated during *C. burnetii* infections, and that the strongest phenotypes are observed at 48 and 72 hours post infection, which is compatible with a reduced, but still detectable translocation of protein to the nucleus at earlier time points. Here we show that indeed the perturbation of nuclear import by NopA affects a broader class of proteins, also outside the

context of *C. burnetii* infections, as indicated by the perturbation of nuclear translocation of IRF3 in response to Sendai Virus infection, in cells ectopically expressing NopA.

To monitor the downstream effects of inhibiting the nuclear accumulation of transcription factors involved in immune sensing, we challenged differentiated THP-1 cells with wt *C. burnetii* or strains carrying mutations either in the Dot/Icm secretion system or in *nopA*. As expected, infections by the wt strain elicited a minor response in the expression of a panel of cytokines, including TNF-α, interleukins and interferons, in agreement with the observation that *C. burnetii* is a stealth pathogen. Evasion of the innate immune response was unmasked by infections with the Dot/Icm-defective strain *dotA*::Tn, which triggered a significant cytokine response. Interestingly, infections by the *nopA*::Tn mutant strain largely phenocopied the *dotA*::Tn mutation, suggesting that NopA is critical for the down-modulation of the innate immune response.

Together, this work highlighted a number of *C. burnetii* eukaryotic-like effector proteins and showed that one of them, NopA, is responsible for evading the host innate immune response by interfering with nucleocytoplasmic transport.

Materials and Methods

Antibodies, reagents, bacterial strains, cell lines and growth conditions used in this study are listed in SI Appendix.

Plasmids.

Plasmids used in this study are listed in Table S4. DNA sequences were amplified by PCR using Phusion polymerase (New England Biolabs) and gene-specific primers (Sigma).

Plasmid design for secretion assay in C. burnetii.

Selected genes from Table S2 were amplified from *C. burnetii* RSA439 NMII genomic DNA using primer pairs indicated in Table S5. PCR products were cloned into the pXDC61-BLAM plasmid to generate N-terminal-tagged fusion version of all candidate effector proteins.

Plasmid design for mammalian cells transfection.

Effector-coding genes were amplified from *C. burnetii* RSA439 NMII genomic DNA using primer pairs indicated in Table S5. PCR products were cloned either into pLVX-mCherry-N2 or pRK5-HA plasmids to generate N-terminal-tagged mCherry or HA fusion versions of all effector proteins, respectively. For tripartite split-GFP assay, pCMV_GFP1-9-OPT, pcDNA3-GFP10-zipper-GFP11, pcDNA3-GFP10-zipper and pcDNA3-zipper-GFP11 were kindly provided by Dr. Stephanie Cabantous. For cloning of Ran in pcDNA3-GFP10-zipper, Ran was amplified using forward primers Ran-BspEI and reverse primers Ran-XbaI-rev. For cloning of NopA, RCC1 and Fibrillarin in pcDNA3-zipper-GFP11, genes were amplified using forward primers NopA-NotI,

RCC1-NotI or FBL-NotI and reverse primers NopA-ClaI-rev, RCC1-ClaI-rev or FBL-ClaI-rev. pGBKT7 containing eukaryotic sequence of Ran WT, RanT24N/Q69L/N122I mutants were kindly provided by Prof. Aymelt Itzen. Ran WT and mutants were amplified from pGBKT7-Ran-WT, pGBKT7-Ran-T24N, pGBKT7-Ran-Q69L, pGBKT7-Ran-N122I using primers pairs XhoI-Ran-F and Ran-XmaI-rev, and the PCR products were cloned into pLVX-GFP-N2.

Plasmid design for nopA complementation in C. burnetii.

For *nopA* complementation, the *nopA* sequence was amplified, together with its putative promoter, using NheI-prom1217-F and PstI-prom1217-R (see Table S5) and the PCR products were cloned into pUC18R6K-miniTn7T-Kan-tetRA-4HA. Plasmids were electroporated in the *nopA*::Tn mutant strain *Tn227* (10).

Beta-Lactamase translocation assay.

For *C. burnetii* effector translocation assays, cells were cultured in black, clear- bottomed, 96-well plates and infected with the appropriate *C. burnetii* strain (MOI of 100) for 24 and 48 h. *C. burnetii* expressing BLAM alone or BLAM-tagged CBU0021 were used as negative and positive controls, respectively. Cell monolayers were loaded with the fluorescent substrate CCF4/AM (LiveBLAzer-FRET B/G loading kit; Invitrogen) in a solution containing 20 mM HEPES, 15 mM probenecid (Sigma) pH 7.3, in HBSS. Cells were incubated in the dark for 1 h at room temperature and imaged using an EVOS inverted fluorescence microscope. Images were acquired using DAPI and GFP filter cubes. The image analysis software CellProfiler was used to segment and count total cells and positive cells in the sample using the 520 nm and 450 nm emission channels, respectively, and to calculate the intensity of fluorescence in each channel.

Following background fluorescence subtraction using negative control samples, the percentage of positive cells was then calculated and used to evaluate effector translocation. A threshold of 20% of positive cells was applied to determine efficient translocation of bacterial effector proteins.

Immunofluorescence staining and microscopy.

Cells were fixed in 4% (wt/vol) paraformaldehyde in PBS solution at room temperature for 20 min. Samples were then rinsed in PBS solution and incubated in blocking solution (0.5% BSA, 50 mM NH_4Cl in PBS solution, pH 7.4). Cells were then incubated with the primary antibodies diluted in blocking solution for 1 h at room temperature, rinsed five times in PBS solution, and further incubated for 1 h with the secondary antibodies diluted in the blocking solution. To visualize HA-tagged NopA or nuclear/nucleolar proteins, cells were fixed as previously described in 4% (wt/vol) paraformaldehyde in PBS solution. Then, cells were permeabilized with 0.5% Triton X-100 in PBS solution for 3 min at room temperature. Sample were then rinsed in PBS solution and incubated with blocking solution [0.1% Triton X-100, 5% (wt/vol) milk in PBS solution] for 1 h at room temperature. Cells were then incubated with the primary antibodies diluted in blocking solution for 1 h at 37 °C, rinsed five times in PBS solution, and incubated with the secondary antibodies for 1 h at room temperature. For all conditions, coverslips were mounted by using Fluoromount mounting medium (Sigma) supplemented with Hoechst 33258 for DNA staining. Samples were imaged with a Zeiss Axio Imager Z1 epifluorescence microscope (Carl Zeiss) connected to a CoolSNAP HQ^2 CCD camera (Photometrics). Images were acquired alternatively with 100x, 63× or 40× oil immersion objectives and processed with MetaMorph (Universal Imaging). ImageJ and CellProfiler software were used for image analysis and quantifications.

568

569 *Immunoprecipitations and pull-down assays.*

570 For coimmunoprecipitation experiments, pLVX-GFP-N2-tagged wt Ran, RanT24N/Q69L/N122I
571 mutants or vector control were co-transfected with pRK5-HA-$NopA_{Cter}$ in U2OS cells. 24 h post
572 transfection, cells were lysed in lysis buffer (10 mM Tris HCl, pH 7.5, 150 mM NaCl, 0.5 mM
573 EDTA, 1% NP-40) supplemented with a protease inhibitor tablet (Complete; Roche) and
574 incubated with 25 µl of GFP-Trap magnetic beads (Chromotek) for 2 h at 4° C with rotation. The
575 beads were then washed 3 times with wash buffer (10 mM Tris HCl, pH 7.5, 150 mM NaCl, 0.5
576 mM EDTA), resuspended in Laemmli buffer 4X and analysed by Western blot.

577

578 *Tripartite split-GFP assay.*

579 U2OS were grown in DMEM supplemented in 10% (v/v) foetal calf serum (FCS) at 37°C and
580 5% CO2. For the interaction assay, U2OS cells were co-transfected with Lipofectamine 2000
581 (Gibco, Invitrogen Co.) with plasmids encoding for GFP1-9, GFP10 and GFP11 fusions. At 24h
582 post transfection, cells were fixed in 4% paraformaldehyde in PBS solution and processed for
583 immunofluorescence. Protein-protein interactions were scored by calculating the percentage of
584 GFP-positive cells over the total number of cells positive for the anti-GFP antibody.

585

586 *Cell fractionation.*

587 U2OS cells were grown to 60% confluence in 100-mm Petri dishes before being transfected with
588 10 µg of pRK5-HA- $NopA_{N\text{-}ter}$ or pRK5-HA- $NopA_{C\text{-}ter}$ in JetPEI reagent (PolyplusTransfection)
589 according to the manufacturer's recommendations. 24 h after transfection, cells were washed in
590 PBS and pelleted at 4°C. U2OS cells cultured in 100-mm dishes were infected with the *nopA*::Tn
591 mutant or the corresponding complemented strain (*nopA*::Tn Comp.) expressing a 4HA-tagged

592 version of NopA. After 24h of infection, cells were washed in PBS and pelleted at 4°C.
593 Transfected or infected cell pellets were subjected to cell fractionation as previously described
594 (37). Where appropriate, cytoplasmic, nuclear and chromatin fractions were subjected to
595 immunoprecipitation using 40 µl of anti-HA magnetic beads (Sigma) for 2 h at 4° C with
596 rotation. Bound proteins were eluted using 80 µl of 100 $\mu g/ml^{-1}$ HA-peptide (Sigma), then
597 resuspended in Laemmli buffer 4X and analysed by Western blot.
598
599 *Ran activation assay.*
600 For the analysis of enzymatic activity of NopA, U2OS cells were either infected or transfected
601 and lysed with lysis buffer (25 mM HEPES, pH 7.5, 150 mM NaCl, 1% NP-40, 10 mM $MgCl_2$, 1
602 mM EDTA, 2% Glycerol) containing a protease inhibitor tablet (Complete; Roche). Cell lysates
603 were then centrifuged for 10 min at 14,000g at 4° C. For Ran-GTP immunoprecipitation, 40 µl of
604 RanBP1 beads (Cell Biolabs, Inc.) were incubated with cell lysates for 1 h at 4° C, and then
605 washed 3 times with lysis buffer, subjected to SDS-PAGE and visualised by Western blotting
606 using an anti-Ran antibody (1:4000, Sigma). GTP-bound Ran levels were determined by
607 calculating the signal ratio of GTP-bound Ran over the total amount of Ran.
608
609 *NF-κB/IRF3 translocation assays.*
610 To analyse NF-κB translocation, U2OS cells were grown to 60% confluence before being
611 transfected as previously described. At 24h post transfection, cells were incubated with media
612 containing 10 ng/ml TNFα for 30min at 37° C. Alternatively, cells were preincubated with media
613 containing 5 nM LMB for 4 hours at 37° C, followed by a TNFα treatment as indicated above
614 where needed. For *C. burnetii* infection assays, cells were infected with *C. burnetii* and incubated

615 at 37° C for 1 to 3 days. Cells were then fixed in 4% paraformaldehyde in PBS solution and
616 processed for NF-κB immunostaining. The image analysis software CellProfiler was used to
617 segment all nuclei using the Hoechst staining and cell contours using nuclei as seeds and the p65
618 labelling. Cytoplasm was segmented by subtracting nuclei from cell objects. Next, mCherry
619 signal was used to identify and isolate the subpopulation of transfected cells, and single cell
620 measurements of the ratio of the mean p65 fluorescence in the nucleus versus cytoplasm were
621 calculated for each condition. For infection assays, CellProfiler was used to identify and isolate
622 the population of infected cells based on the GFP fluorescence associated with the strains of
623 *C. burnetii* used in this study and nuclear p65 fluorescence was specifically measured as
624 described above in the subpopulation of infected cells. To analyse IRF3 translocation, pLVX-
625 mCherry-N2-tagged NopA, CvpB or empty vector were co-transfected with pcDNA3-3xFLAG-
626 tagged IRF-3 in U2OS cells. At 24h post transfection, cells were infected with a defective-
627 interfering H4 Sendai Virus (38) provided by D. Garcin (Department of Microbiology and
628 Molecular Medicine, University of Geneva, Switzerland) and used at 50 hemagglutination units
629 HAU/ml for 18h at 37°C. Cells were then fixed in 4% paraformaldehyde in PBS solution and
630 processed for FLAG immunostaining. IRF3 nuclear translocation was measured as described
631 above for p65.
632
633 *Densitometry.*
634 Regions of Interest (ROIs) were obtained from each band of interest and the intensity was
635 measured using ImageJ. For each band, the same ROI was used for background calculation and
636 removal from areas adjacent to each band. For the experiments illustrated in Figure 5, the
637 intensity of bands from samples treated with TNF were normalised for the intensity of the

638 corresponding untreated sample. For the experiments illustrated in Figure 6, the intensity of
639 bands from samples challenged with *C. burnetii* or treated with TNF were normalised for the
640 intensity of the non-infected (NI) sample.
641
642 *Real-time quantitative RT-PCR (qRT-PCR) analysis of cytokine mRNA.*
643 Total RNA was extracted from THP-1 cells using the RNeasy Micro kit and was submitted to
644 DNase treatment (Qiagen), following manufacturer's instructions. RNA concentration and purity
645 were evaluated by spectrophotometry (NanoDrop 2000c, Thermo Fisher Scientific). 500 ng of
646 RNA were reverse transcribed with both oligo-dT and random primers, using PrimeScript RT
647 Reagent Kit (Perfect Real Time, Takara) in a 10 ml reaction. Real time PCR reactions were
648 performed in duplicates using Takyon ROX SYBR MasterMix blue dTTP (Eurogentec) on an
649 Applied Biosystems QuantStudio 5, using the following program: 3 min at 95°C followed by 40
650 cycles of 15 s at 95°C, 20 s at 60°C and 20 s at 72°C. Ct values for each transcript were
651 normalised to the geometric mean of the expression of RPL13A, B2M and ACTB (i.e. reference
652 genes) and the fold-changes were determined by using the $2^{-\Delta\Delta Ct}$ method. Primers used for
653 quantification of transcripts by real time quantitative PCR are indicated in Table S5.
654
655 *SCID mouse infections.*
656 SCID (C.B-17/LcrHsd-Prkdcscid) mice were purchased from Envigo (Indianapolis, IN, USA)
657 and housed in the TAMHSC animal facility. All animal procedures were done in compliance with
658 Texas A&M University IACUC (AUP#2016-0370). Infections were performed as described
659 previously (36). Briefly, 6-8 week old female mice (SCID or C57BL/6) were infected with 1 x
660 10^6 viable *C. burnetii* phase II strain via intra-peritoneal (IP) injection. Inoculum concentrations
661 were confirmed by serial dilution spot plating on ACCM-D agarose as described previously (39).

662

663 *Mouse tissue collection, processing, and DNA purification.*

664 At 10 days (competitive infections) or 14 days post-infection (single infections), the mouse
665 spleens were removed and weighed at necropsy to determine splenomegaly (spleen weight/body
666 weight). Each spleen was added to 1 mL PBS and homogenized using an Omni (TH) equipped
667 with plastic tips (Kennesaw, GA, USA). 100 μL of homogenate was added to 400 μL of TriZol
668 LS (Invitrogen) for RNA extraction. For DNA extraction, 100 μL of homogenate was added to
669 900 μL tissue lysis buffer (Roche) plus 100 μL of proteinase K and incubated at 55ºC overnight.
670 The following day 100 μL of 10% SDS (w/v) was added and incubated at room temperature for 1
671 hour. Lysed tissue samples were then processed using Roche High Pure PCR template
672 preparation kit according to manufacturer's instructions (Indianapolis, IN, USA).

673

674 *Enumeration of Coxiella in Mouse Spleens.*

675 DNA purified from infected organs was used as template for TaqMan real time PCR using
676 primers and probe for *com1* or primers and probe of *IS1111* as described previously (36).
677 Quantitative PCR was performed in 20 μL reactions with ABI TaqMan universal PCR mastermix
678 run on an ABI StepOne Plus machine. The replication index reported for each mouse was
679 calculated by dividing the number of genome copies recovered from spleens by the number of
680 genome copies in the original inoculum.

681

682 *Flow cytometry.*

683 For intracellular human TNF-α/IFN-α4 staining, 5 x 10^4 THP-1 cells differentiated in PMA (200
684 ng/mL) for 2 day seeded in 24-well plates were infected with the indicated *C. burnetii* strain for

72 and 96 h. Cells were then treated with 1 μg/ml of brefeldin A (BFA) for the last 24 hours. The following day, cells were fixed using 2% paraformaldehyde in PBS solution for 20 min at 4° C. After washing with FACS buffer (1% BSA in PBS solution), cells were permeabilized in FACS buffer supplemented with 0.1% saponin for 30 min at 4° C and then stained with anti-TNF-α-PE and IFN-α-PE antibodies for 1 hour at 4° C. Infected cells were analysed based on the GFP fluorescence associated with the strains of *C. burnetii*. Flow cytometry analyses were performed on a BD FACSCalibur flow cytometer using flow cytometry (CellQuest software, BD Biosciences, San Jose, CA). FlowJo software (Tree Star, Ashland, OR) was used to analyze data.

Data Availability Statement: All data discussed in the paper will be made available to readers.

Acknowledgements

This work was supported by the ERA-NET Infect-ERA (ANR-13-IFEC-0003), the French National Research Agency (ANR; ANR-14-CE14-0012-01, ANR-10-LABX-12-01). GM is the recipient of a fellowship from the Agence National de la Recherche sur le SIDA et les Hépatites virales (ANRS). We acknowledge the imaging facility MRI, member of the national infrastructure France-BioImaging supported by the French National Research Agency (ANR-10-INBS-04, «Investments for the future»). We thank Dr Caroline Goujon, Dr Marylene Mougel (IRIM, Montpellier, France), Prof. Hubert Hilbi and Leoni Swart (University of Zurich, Switzerland), and Prof. Aymelt Itzen (University of Hamburg, Germany) for scientific advice and sharing material.

Declaration of interest statement

The authors declare no conflicts of interest.

Figure Legends

Figure 1. Identification of *C. burnetii* EUGENs. **A**, U2OS cells were challenged with *C. burnetii* strains expressing BLAM-tagged versions of candidate EUGENs for 6, 12, 24, 48 and 72 hours. The percentage of BLAM-positive, infected cells was automatically calculated using CellProfiler over the total number of infected cells per each condition. Empty = BLAM empty vector. The Dot/Icm-dependent translocation of the effectors that were efficiently secreted was validated in the *dotA*::Tn mutant strain at 72 hours post challenge. **B**, Representative images of positive (blue) cells treated as in **A**. **C**, Non-infected or GFP-expressing *C. burnetii*-infected U2OS cells were transfected with plasmids encoding N-terminally tagged mCherry versions of the effector proteins validated in **A** (red). 24 hours after transfection cells were fixed and labelled with Hoechst (blue) and an anti-LAMP1 antibody (white). White arrows point at CBU1217 sub-nuclear localisation. Scale bars are 10 μm.

Figure 2. Intracellular localisation of CBU1217/NopA and role in *C. burnetii* replication during infection. U2OS cells were challenged either with wt GFP-tagged *C. burnetii* (white) transformed with plasmids encoding 4HA-tagged CBU1217/NopA (**A**, **B**, red) or the 4HA tag alone (**C**, red), or with the GFP-tagged *dotA*::Tn mutant (**D**, white), transformed with plasmids encoding 4HA-tagged CBU1217/NopA, all under the control of an IPTG-inducible promoter. 72 hours post-infection cells were fixed and labelled with Hoechst (blue) and anti-fibrillarin antibodies (green). I= IPTG-induced; NI= non-induced. Arrow points at 4HA-CBU1217/NopA localisation in infected cell. U2OS cells were transfected with plasmids encoding HA-tagged versions of either full length (**E**), or the indicated deletion mutants (**F** and **G**) of HA-tagged NopA. 24 hours after transfection cells were either fixed and labelled with Hoechst (blue), an

anti-fibrillarin antibody (green) and an anti-HA antibody (red, centre panels) or lysed and processed for cell fractionation (right panels). Cell fractions were analysed by Western blotting using anti-fibrillarin and anti-GAPDH antibodies as nuclear and chromatin (Nu, Ch) and cytoplasmic (Cy) markers, respectively, and anti-HA antibodies to reveal NopA localisation. Scale bars are 10 μm. **H**, Genome Equivalents (GE) calculated using TaqMan real-time PCR with DNA purified from infected spleens of 5 SCID mice per group on day 14 after challenge with $1x10^6$ GE of the strains shown. **I**, Replication index calculated as the ratio between spleen GE at the time of necropsy and the input GE of the strains listed in the figure legend. **J**, Spleen weight as a percentage of total body weight at the time of necropsy on day 14 after infection with $1x10^6$ GE of the strains listed in the figure legend. Values are the mean of three independent infections, with error bars indicating standard deviations from the mean.

Figure 3. NopA interacts with the small GTPase Ran. A, U2OS cells challenged for 24 hours with either the *C. burnetii nopA* transposon mutant (*nopA*::Tn) or the corresponding complemented strain (*nopA*::Tn Comp.) were lysed and processed for cell fractionation. Whole cell lysates (WCL) were probed with the indicated antibodies, as well as anti-GAPDH and anti-fibrillarin antibodies as cytoplasmic (Cy), and nuclear/chromatin (Nu, Ch) markers, respectively. Following immunoprecipitation with anti-HA-coated magnetic beads, the presence of Ran and that of fibrillarin (as a negative control) was assessed using specific antibodies (IP HA). **B**, U2OS cells transfected with HA-tagged versions of either the N-terminal domain ($NopA_{N\text{-}ter}$), the C-terminal domain ($NopA_{C\text{-}ter}$) of NopA or CvpF as negative control were lysed and processed for cell fractionation. Whole cell lysates (WCL) were probed with the indicated antibodies, as well as anti-GAPDH and anti-fibrillarin antibodies as cytoplasmic (Cy), nuclear/chromatin (Nu, Ch)

markers, respectively. Following immunoprecipitation with anti-HA-coated magnetic beads, the presence of candidate interacting proteins was assessed using specific antibodies (IP HA). **C**, U2OS cells were transfected with plasmids encoding GFP1-9 in combination with plasmids encoding either the GFP10 and GFP11 tags alone as negative control (top row), GFP10 and GFP11 linked by a leucine zipper motif (GFP10-zip-GFP11) as positive control (middle row) or GFP10-Ran and GFP11-NopA (bottom row). 24 hours after transfection cells were fixed and labelled with Hoechst (blue) and anti-GFP antibodies (red) to reveal nuclei and the expression of GFP1-9, respectively. Protein-protein interaction was assessed following the reconstitution of GFP (Reconst. GFP, green). **D**, the percentage of cells presenting GFP reconstitution over the total number of GFP1-9-positive cells was calculated. Values are means ± SD from 2 independent experiments. Asterisks indicate statistically significant variations (n.s. = non-significant, **** = P<0.0001, one-way ANOVA, Dunnett's multiple comparison test). Scale bars are 20 μm.

Figure 4. NopA increases the intracellular levels of Ran-GTP. A, The GFP-trap assay was carried out in U2OS cells expressing HA-tagged $NopA_{C\text{-}ter}$ in combination with either GFP alone, GFP-Ran, GFP-Ran_{T24N} (GDP-locked), GFP-Ran_{Q69L} (GTP-locked) or GFP-Ran_{N122I} (guanosine free). Whole cell lysates (WCL, upper panels) were probed with anti-GFP and anti-HA antibodies to assess the expression of the GFP-tagged proteins and HA-tagged $NopA_{C\text{-}ter}$, and anti-tubulin antibodies as loading control. Protein-protein interactions were assessed using anti-GFP and anti-HA antibodies following GFP capture (GFP-trap, lower panels). **B**, GTP-bound Ran was pulled down using RanBP1-coated beads from cell lysates of U2OS cells challenged for 24 hours with either wt *C. burnetii* (wt), a *nopA* transposon mutant (*nopA*::Tn), the corresponding

complemented strain (*nopA*::Tn Comp.) or the Dot/Icm-defective mutant (*dotA*::Tn). Non-infected cells were used as control. Whole cell lysates (WCL) were probed with anti-*C. burnetii* (NMII), anti-Ran and anti-β-tubulin antibodies. GTP-bound Ran was revealed using an anti-Ran antibody (IP RanBP1). **C**, GTP-bound Ran was pulled down using RanBP1-coated beads from cell lysates of U2OS cells expressing either the HA tag alone, HA-tagged versions of either full length ($NopA_{FL}$), the N-terminal domain ($NopA_{N\text{-}ter}$), the C-terminal domain ($NopA_{C\text{-}ter}$) of NopA or CvpB. Whole cell lysates (WCL) were probed with anti-HA antibodies to assess the expression of the HA-tagged versions of NopA and anti-Ran and anti-tubulin antibodies as loading controls. GTP-bound Ran was revealed using an anti-Ran antibody (IP RanBP1). The signal ratio of GTP-bound Ran over the total amount of Ran is indicated for experiments illustrated in **B** and **C**. Values are mean ± SD from 3 independent experiments. n.s = non-significant, **** = P<0.0001, ** = P<0.007, * = P<0.02, one-way ANOVA, Dunnett's multiple comparison test.

Figure 5. Overexpression of NopA interferes with the nuclear translocation of p65. Representative Western blot of U2OS cells expressing either the HA tag alone, HA-NopA or HA-CvpB left untreated or incubated with 10 ng/ml TNF-α for 30 min, lysed and processed for cell fractionation. Whole cell lysates (**A**, WCL) were used to assess the overall levels of p65 and IκBα and nuclear fractions (**B**) to monitor p65 translocation to the nucleus (Nuclear Fraction). The signal ratio of p65 over tubulin or fibrillarin and of IκBα over tubulin is indicated for experiments illustrated in **A** and **B**. Values are mean ± SD from 3 independent experiments. **C**, Representative images of U2OS cells expressing mCherry-NopA or mCherry-CvpB and treated as in **A**. The localisation of p65 was monitored using an anti-p65 antibody and Hoechst staining

of nuclei. Asterisks indicate transfected cells. **D**, CellProfiler was used to identify mCherry-expressing U2OS cells and measure the median of the ratios of p65 fluorescence intensity at nuclei versus cytoplasm. Values are means ± SEM from 2 independent experiments where a minimum of 200 nuclei were measured per condition. Asterisks indicate statistically significant variations (n.s. = non-significant, **** = P<0.0001, *** = P<0.001, ** = P<0.01, * = P<0.1, one-way ANOVA, Dunnett's (A & B) and Bonferroni (D) multiple comparison test). Scale bars are 10 μm.

Figure 6. NopA interferes with the nuclear translocation of p65 during *C. burnetii* infections. Representative Western blot of U2OS cells challenged for 72 hours with GFP-tagged strains of wt *C. burnetii* (wt), the Dot/Icm-defective *dotA* transposon mutant (*dotA*::Tn), the *nopA* transposon mutant (*nopA*::Tn) or the corresponding complemented strain (*nopA*::Tn Comp.). Non-infected cells (NI) and cells treated with 10 ng/ml TNF-α (TNF-α) for 30 min were used as negative and positive controls, respectively. Cells were lysed and fractionated to isolate nuclear fractions. Whole cell lysates (**A**, WCL) were used to assess the overall levels of p65 and IκBα and nuclear fractions (**B**) to monitor p65 translocation to the nucleus (Nuclear Fraction). Normalised densitometry of indicated protein ratios was calculated. Values are means ± SD from 2 independent experiments. **C**, Representative images of U2OS cells treated as in **A**. The localisation of p65 (red) was monitored using an anti-p65 antibody and Hoechst staining of nuclei (blue). White arrows indicate nuclei of infected cells. **D**, U2OS cells were treated as in **A** for 24, 48 and 72 hours. CellProfiler was used to identify infected and total U2OS cells and measure the median of the ratios of p65 fluorescence intensity at nuclei versus cytoplasm. Values are means ± SEM from 2 independent experiments where a minimum of 400 nuclei were measured per

condition (n.s. = non-significant, *** = P<0.0001, one-way ANOVA, Dunnett's multiple comparison test). Scale bars are 10 μm.

Figure 7. NopA inhibits cytokines production. A, Differentiated THP-1 cells were challenged either with GFP-expressing wt *C. burnetii* (wt), the Dot/Icm-defective *dotA* transposon mutant (*dotA*::Tn), the *nopA* transposon mutant (*nopA*::Tn) or the corresponding complemented strain (*nopA*::Tn Comp.) for 24, 48, 72 and 96 hours. The expression of TNF-α and IFN-α4 cytokines was assessed by RT-qPCR for the indicated time points. **B**, Dot plots from a representative experiment showing intracellular staining of TNF-α and IFN-α in cells infected for 72 and 96 hours and treated with brefeldin A (BFA) for the last 24 hours. Infected cells were first gated on GFP+ population and the percentage of cells expressing TNF-α and IFN-α was assessed. Flow cytometry data are presented on graphs as fold relative to wt. Values are means ± SD from three independent experiments. n.s. = non-significant, **** = P<0.0001, *** = P<0.001, ** = P<0.01, * = P<0.1. Full statistical analysis for the 72 hours time point illustrated in **A** is available at Figure S7.

Supplementary figure legends are available in SI Appendix

References

1. M. M. Rahman, G. McFadden, Modulation of NF-κB signalling by microbial pathogens. *Nat. Rev. Microbiol.* **9**, 291–306 (2011).
2. S. Asrat, K. M. Davis, R. R. Isberg, Modulation of the host innate immune and inflammatory response by translocated bacterial proteins. *Cell. Microbiol.* **17**, 785–795 (2015).
3. M. Stewart, Molecular mechanism of the nuclear protein import cycle. *Nat. Rev. Mol. Cell Biol.* **8**, 195–208 (2007).
4. N. Rolhion, *et al.*, Inhibition of Nuclear Transport of NF-κB p65 by the Salmonella Type III Secretion System Effector SpvD. *PLoS Pathog.* **12**, 1–26 (2016).
5. S. M. Evans, K. G. Rodino, H. E. Adcox, J. A. Carlyon, *Orientia tsutsugamushi* uses two Ank effectors to modulate NF-κB p65 nuclear transport and inhibit NF-κB transcriptional activation. *PLoS Pathog.* **14**, 1–39 (2018).
6. A. Lührmann, H. J. Newton, M. Bonazzi, Beginning to understand the role of the Type IV secretion system effector proteins in *Coxiella burnetii* pathogenesis. *Curr. Top. Microbiol. Immunol.* **413**, 243–268 (2017).
7. C. L. Larson, *et al.*, Right on Q: Genetics begin to unravel *Coxiella burnetii* host cell interactions. *Future Microbiol.* **11**, 919–939 (2016).
8. L. D. Cunha, *et al.*, Inhibition of inflammasome activation by *Coxiella burnetii* type IV secretion system effector IcaA. *Nat. Commun.* **6**, 10205 (2015).
9. S. Mahapatra, *et al.*, *Coxiella burnetii* Employs the Dot/Icm Type IV Secretion System to Modulate Host NF-κB/RelA Activation. *Front. Cell. Infect. Microbiol.* **6**, 1–13 (2016).
10. E. Martinez, F. Cantet, L. Fava, I. Norville, M. Bonazzi, Identification of OmpA, a *Coxiella burnetii* Protein Involved in Host Cell Invasion, by Multi-Phenotypic High-

Content Screening. *PLoS Pathog.* **10**, e1004013 (2014).

11. E. Martinez, F. Cantet, M. Bonazzi, Generation and multi-phenotypic high-content screening of *Coxiella burnetii* transposon mutants. *J. Vis. Exp.* **2015** (2015).

12. E. Martinez, *et al.*, *Coxiella burnetii* effector CvpB modulates phosphoinositide metabolism for optimal vacuole development. *Proc. Natl. Acad. Sci.* **113**, E3260–E3269 (2016).

13. O. Hadjebi, E. Casas-Terradellas, F. R. Garcia-Gonzalo, J. L. Rosa, The RCC1 superfamily: from genes, to function, to disease. *Biochim. Biophys. Acta* **1783**, 1467–79 (2008).

14. T. Seki, N. Hayashi, T. Nishimoto, RCC1 in the Ran pathway. *J. Biochem.* **120**, 207–214 (1996).

15. L. Renault, *et al.*, The 1.7 Å crystal structure of the regulator of chromosome condensation (RCC1) reveals a seven-bladed propeller. *Nature* **392**, 97–101 (1998).

16. C. Noroy, T. Lefrançois, D. F. Meyer, Searching algorithm for Type IV effector proteins (S4TE) 2.0: Improved tools for Type IV effector prediction, analysis and comparison in proteobacteria. *PLoS Comput. Biol.* **15**, e1006847 (2019).

17. X. Pan, A. Lührmann, A. Satoh, M. A. Laskowski-Arce, C. R. Roy, Ankyrin repeat proteins comprise a diverse family of bacterial type IV effectors. *Science (80-.).* **320**, 1651–1654 (2008).

18. D. E. Voth, *et al.*, The *Coxiella burnetii* ankyrin repeat domain-containing protein family is heterogeneous, with C-terminal truncations that influence Dot/Icm-mediated secretion. *J. Bacteriol.* **191**, 4232–4242 (2009).

19. C. Chen, *et al.*, Large-scale identification and translocation of type IV secretion substrates by *Coxiella burnetii*. *Proc. Natl. Acad. Sci.* **107**, 21755–21760 (2010).

20. K. L. Carey, H. J. Newton, A. Lührmann, C. R. Roy, The *Coxiella burnetii* Dot/Icm System Delivers a Unique Repertoire of Type IV Effectors into Host Cells and Is Required for Intracellular Replication. *PLoS Pathog.* **7**, e1002056 (2011).

21. R. A. Eckart, *et al.*, Antiapoptotic Activity of *Coxiella burnetii* Effector Protein AnkG Is Controlled by p32-Dependent Trafficking. *Infect. Immun.* **82**, 2763–2771 (2014).

22. F. A. Siadous, F. Cantet, E. van Schaik, M. Burette, J. Allombert, A. Lakhani, B. Bonaventure, C. Goujon, J.E. Samuel, M. Bonazzi, E. Martinez. *Coxiella* effector protein CvpF subverts RAB26-dependent autophagy to promote vacuole biogenesis and virulence. *Autophagy* (2020, *in press*)

23. S. Cabantous, *et al.*, A New Protein-Protein Interaction Sensor Based on Tripartite Split-GFP Association. *Sci. Rep.* **3**, 2854 (2013).

24. I. Palacios, K. Weis, C. Klebe, I. W. Mattaj, C. Dingwall, RAN/TC4 mutants identify a common requirement for snRNP and protein import into the nucleus. *J. Cell Biol.* (1996).

25. E. M. Campoy, F. C. M. Zoppino, M. I. Colombo, The Early Secretory Pathway Contributes to the Growth of the *Coxiella* -Replicative Niche. *Infect. Immun.* **79**, 402–413 (2011).

26. K. S. De Felipe, *et al.*, Evidence for acquisition of *Legionella* type IV secretion substrates via interdomain horizontal gene transfer. *J. Bacteriol.* **187**, 7716–7726 (2005).

27. K. S. De Felipe, *et al.*, *Legionella* eukaryotic-like type IV substrates interfere with organelle trafficking. *PLoS Pathog.* **4** (2008).

28. M. Ohtsubo, H. Okazaki, T. Nishimoto, The RCC1 protein, a regulator for the onset of chromosome condensation locates in the nucleus and binds to DNA. *J. Cell Biol.* **109**, 1389–1397 (1989).

29. I. G. M. Michael E. Nemergut, Craig A. Mizzen, Todd Stukenberg, C. David Allis, The,

Chromatin Docking and Exchange Activity Enhancement of RCCl by Histones H2A and H2B. **292**, 1540–1543 (2001).

30. P. R. Clarke, C. Zhang, Spatial and temporal coordination of mitosis by Ran GTPase. *Nat. Rev. Mol. Cell Biol.* **9**, 464–477 (2008).

31. S. Ninio, J. Celli, C. R. Roy, A *Legionella pneumophila* effector protein encoded in a region of genomic plasticity binds to Dot/Icm-modified vacuoles. *PLoS Pathog.* **5** (2009).

32. E. Rothmeier, *et al.*, Activation of Ran GTPase by a *Legionella* Effector Promotes Microtubule Polymerization, Pathogen Vacuole Motility and Infection. *PLoS Pathog.* **9** (2013).

33. W. Schäfer, *et al.*, Nuclear trafficking of the anti-apoptotic *Coxiella burnetii* effector protein AnkG requires binding to p32 and Importin-α1. *Cell. Microbiol.* **19** (2017).

34. M. M. Weber, *et al.*, Modulation of the host transcriptome by *Coxiella burnetii* nuclear effector Cbu1314. *Microbes Infect.* **18**, 336–345 (2016).

35. A. Chong, *et al.*, The early phagosomal stage of *Francisella tularensis* determines optimal phagosomal escape and *Francisella* pathogenicity island protein expression. *Infect. Immun.* (2008)

36. E. J. van Schaik, E. D. Case, E. Martinez, M. Bonazzi, J. E. Samuel, The SCID mouse model for identifying virulence determinants in *Coxiella burnetii*. *Front. Cell. Infect. Microbiol.* **7**, 1–10 (2017).

37. A. Prokop, *et al.*, Orfx, a nucleomodulin required for listeria monocytogenes virulence. *MBio* **8** (2017).

38. L. Strahle, D. Garcin, D. Kolakofsky, Sendai virus defective-interfering genomes and the activation of interferon-beta. *Virology* **351**, 101–111 (2006).

39. K. M. Sandoz, P. A. Beare, D. C. Cockrell, R. A. Heinzen, Complementation of Arginine

Auxotrophy for Genetic Transformation of *Coxiella burnetii* by Use of a Defined Axenic Medium. *Appl. Environ. Microbiol.* **82**, 3695–3695 (2016).

Figure 1

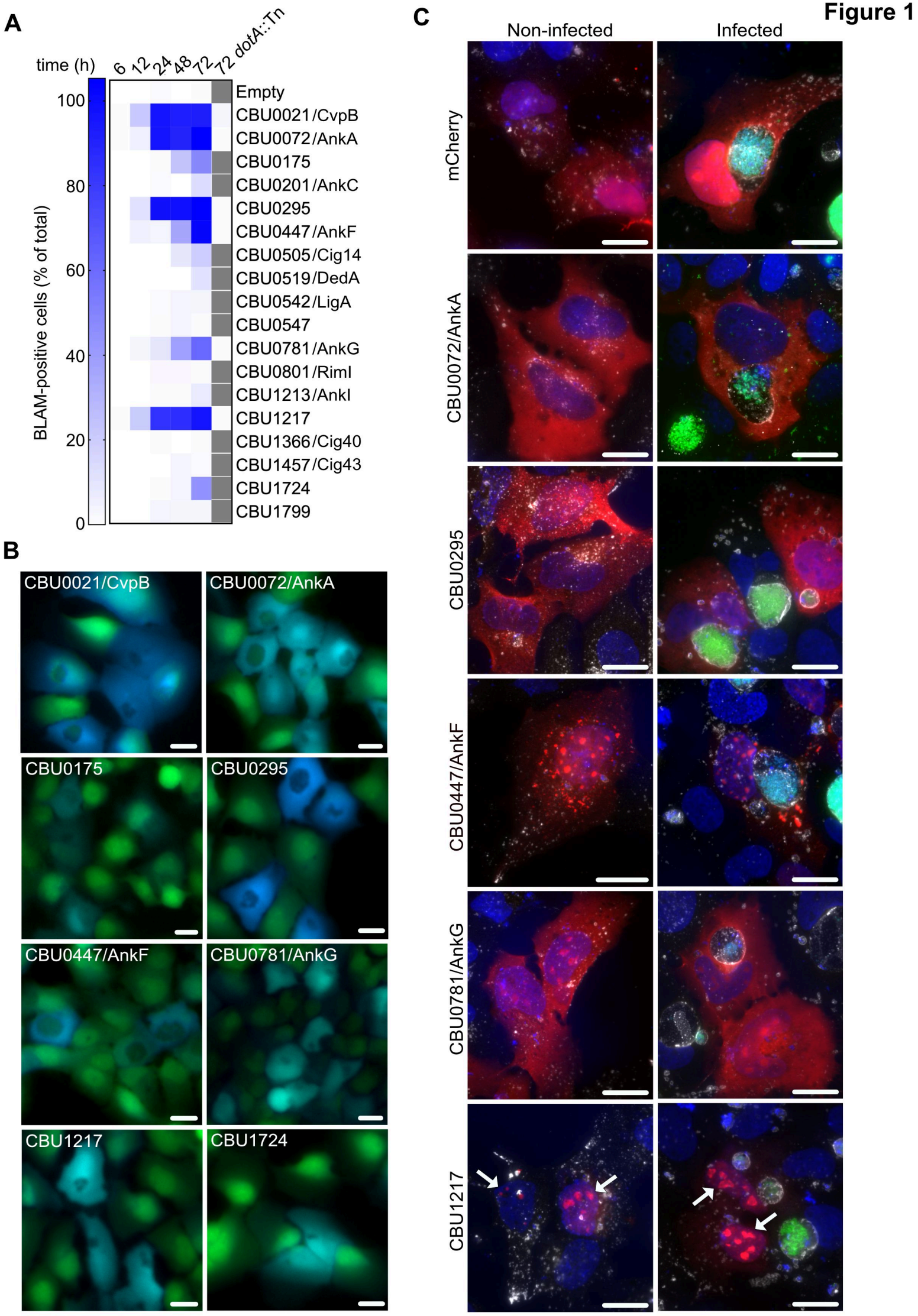
A
time (h)
6
12
24
48
72
72 dotA::Tn
Empty
CBU0021/CvpB
CBU0072/AnkA
CBU0175
CBU0201/AnkC
CBU0295
CBU0447/AnkF
CBU0505/Cig14
CBU0519/DedA
CBU0542/LigA
CBU0547
CBU0781/AnkG
CBU0801/RimI
CBU1213/AnkI
CBU1217
CBU1366/Cig40
CBU1457/Cig43
CBU1724
CBU1799
BLAM-positive cells (% of total)
100
80
60
40
20
0
B
CBU0021/CvpB
CBU0072/AnkA
CBU0175
CBU0295
CBU0447/AnkF
CBU0781/AnkG
CBU1217
CBU1724
C
Non-infected
Infected
mCherry
CBU0072/AnkA
CBU0295
CBU0447/AnkF
CBU0781/AnkG
CBU1217

Figure 2

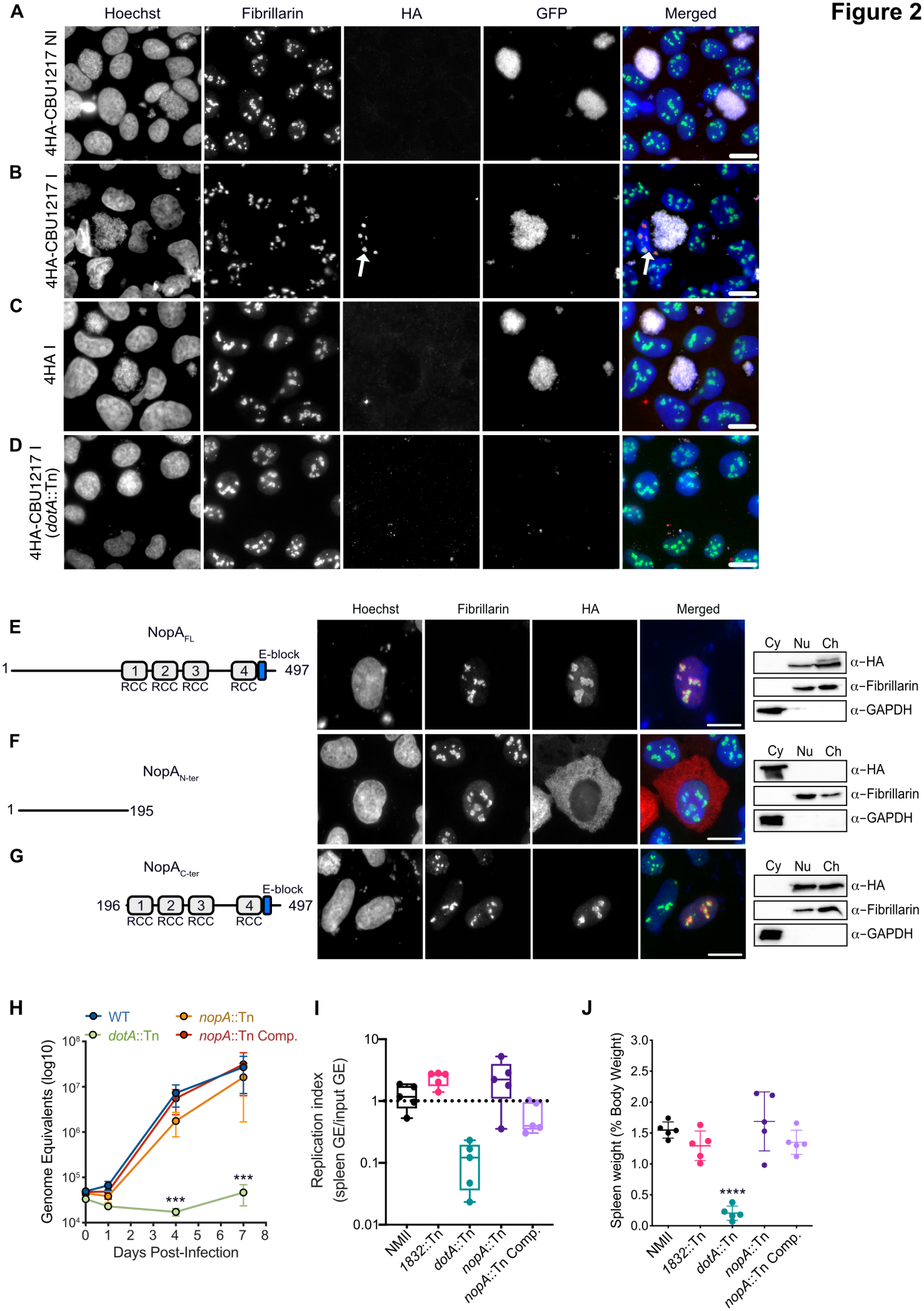
A
Hoechst
Fibrillarin
HA
GFP
Merged
4HA-CBU1217 NI
B
4HA-CBU1217 I
C
4HA I
D
4HA-CBU1217 I (dotA::Tn)
E
NopA$_{FL}$
1
RCC RCC RCC RCC
E-block
497
F
NopA$_{N-ter}$
195
G
NopA$_{C-ter}$
196
Cy Nu Ch
α-HA
α-Fibrillarin
α-GAPDH
H
WT
dotA::Tn
nopA::Tn
nopA::Tn Comp.
Genome Equivalents (log10)
Days Post-Infection
***
I
Replication index (spleen GE/input GE)
NMII
1832::Tn
dotA::Tn
nopA::Tn
nopA::Tn Comp.
J
Spleen weight (% Body Weight)
****

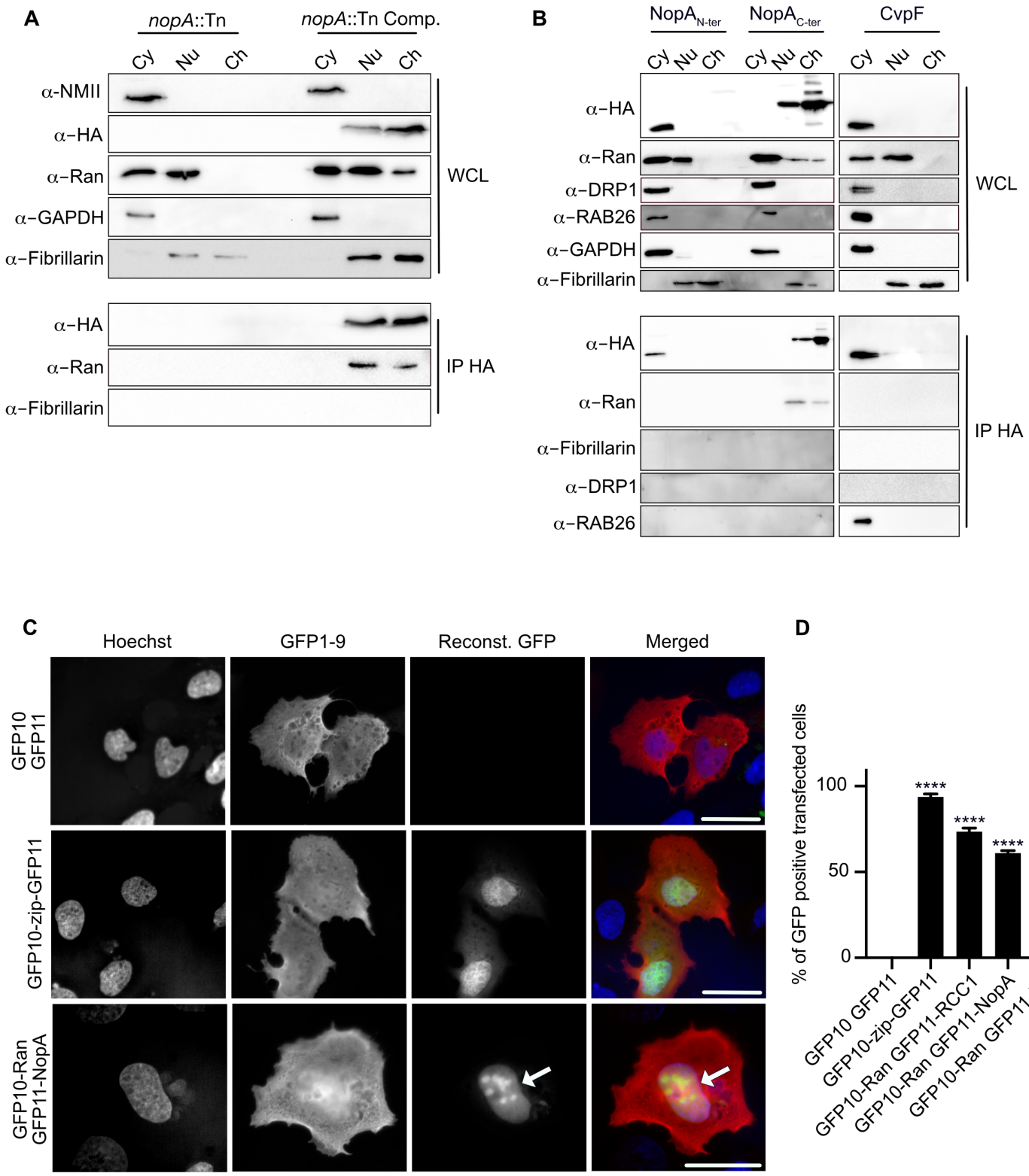
A
nopA::Tn
nopA::Tn Comp.
Cy Nu Ch Cy Nu Ch
α-NMII
α-HA
α-Ran
α-GAPDH
α-Fibrillarin
WCL
α-HA
α-Ran
α-Fibrillarin
IP HA
B
NopA N-ter
NopA C-ter
CvpF
Cy Nu Ch Cy Nu Ch Cy Nu Ch
α-HA
α-Ran
α-DRP1
α-RAB26
α-GAPDH
α-Fibrillarin
WCL
α-HA
α-Ran
α-Fibrillarin
α-DRP1
α-RAB26
IP HA
C
Hoechst
GFP1-9
Reconst. GFP
Merged
GFP10 GFP11
GFP10-zip-GFP11
GFP10-Ran GFP11-NopA
D
% of GFP positive transfected cells
100
50
0
****
****
****
n.s.
GFP10 GFP11
GFP10-zip-GFP11
GFP10-Ran GFP11-RCC1
GFP10-Ran GFP11-NopA
GFP10-Ran GFP11-Fib

Figure 4

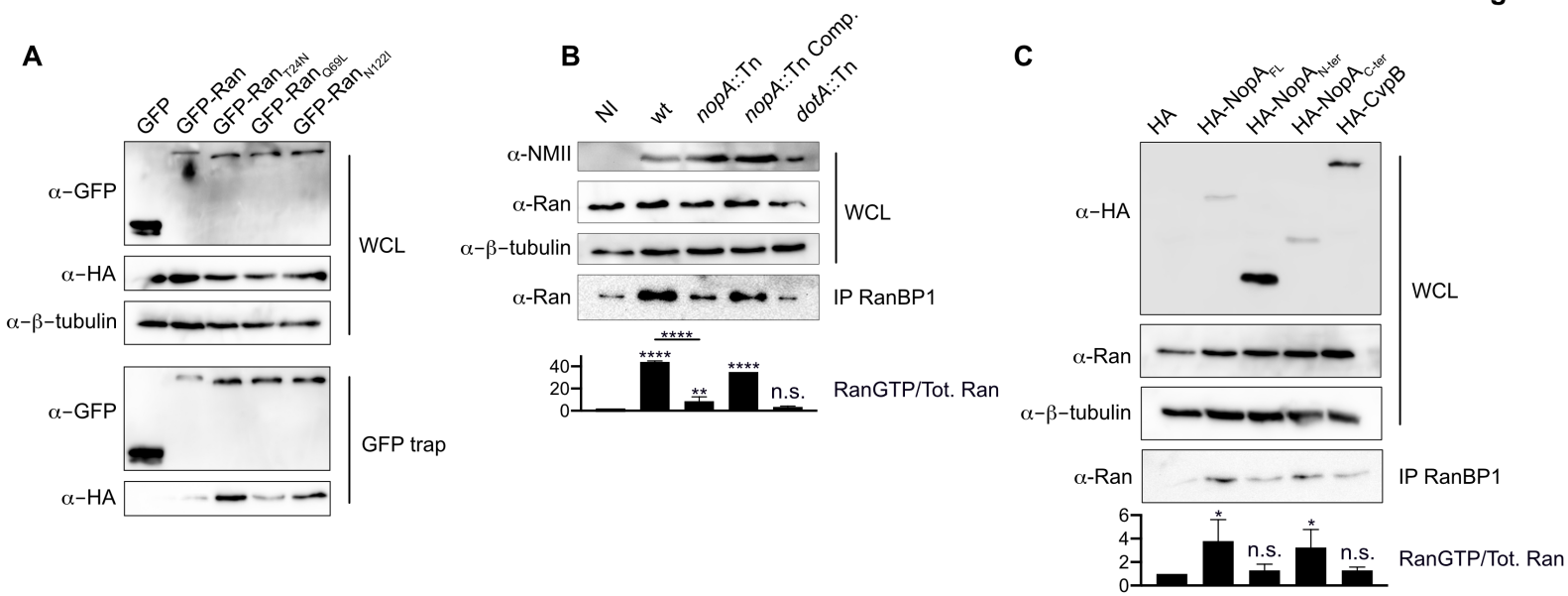
A
GFP
GFP-Ran
GFP-Ran T24N
GFP-Ran Q69L
GFP-Ran N122I
α−GFP
α−HA
α−β−tubulin
WCL
α−GFP
α−HA
GFP trap
B
NI
wt
nopA::Tn
nopA::Tn Comp.
dotA::Tn
α-NMII
α-Ran
α−β−tubulin
WCL
α-Ran
IP RanBP1
****
****
**
****
n.s.
40
20
0
RanGTP/Tot. Ran
C
HA
HA-NopA FL
HA-NopA N-ter
HA-NopA C-ter
HA-CvpB
α−HA
WCL
α-Ran
α−β−tubulin
α-Ran
IP RanBP1
6
4
2
0
*
n.s.
*
n.s.
RanGTP/Tot. Ran

Figure 5

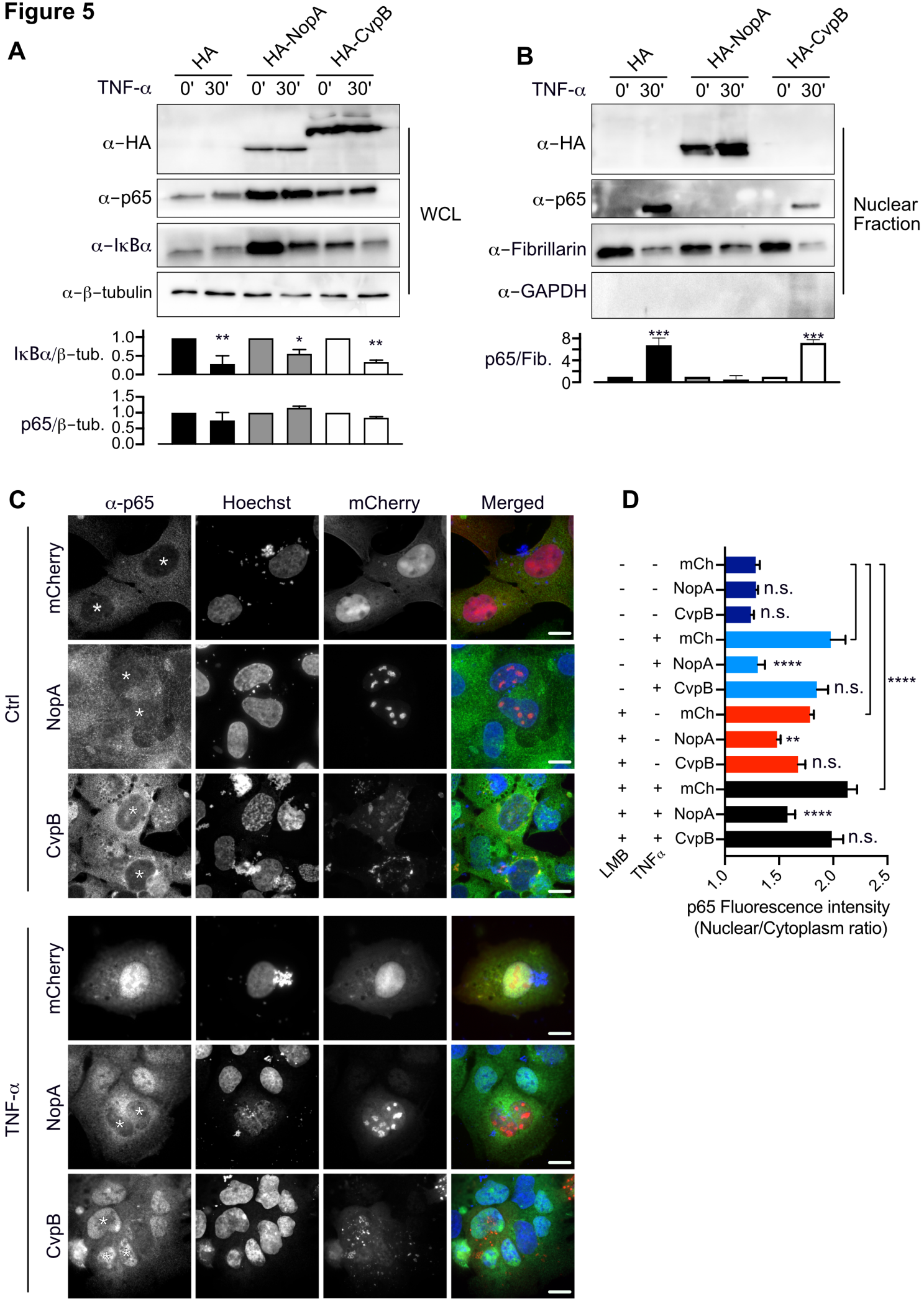
A
HA
HA-NopA
HA-CvpB
TNF-α
0' 30' 0' 30' 0' 30'
α-HA
α-p65
α-IκBα
α-β-tubulin
WCL
IκBα/β-tub.
1.0
0.5
0.0
**
*
**
p65/β-tub.
1.5
1.0
0.5
0.0
B
HA
HA-NopA
HA-CvpB
TNF-α
0' 30' 0' 30' 0' 30'
α-HA
α-p65
α-Fibrillarin
α-GAPDH
Nuclear Fraction
p65/Fib.
8
4
0
***
***
C
α-p65
Hoechst
mCherry
Merged
Ctrl
mCherry
NopA
CvpB
TNF-α
mCherry
NopA
CvpB
D
- - mCh
- - NopA n.s.
- - CvpB n.s.
- + mCh
- + NopA ****
- + CvpB n.s.
+ - mCh
+ - NopA **
+ - CvpB n.s.
+ + mCh
+ + NopA ****
+ + CvpB n.s.
****
LMB
TNFα
1.0
1.5
2.0
2.5
p65 Fluorescence intensity
(Nuclear/Cytoplasm ratio)

Figure 6

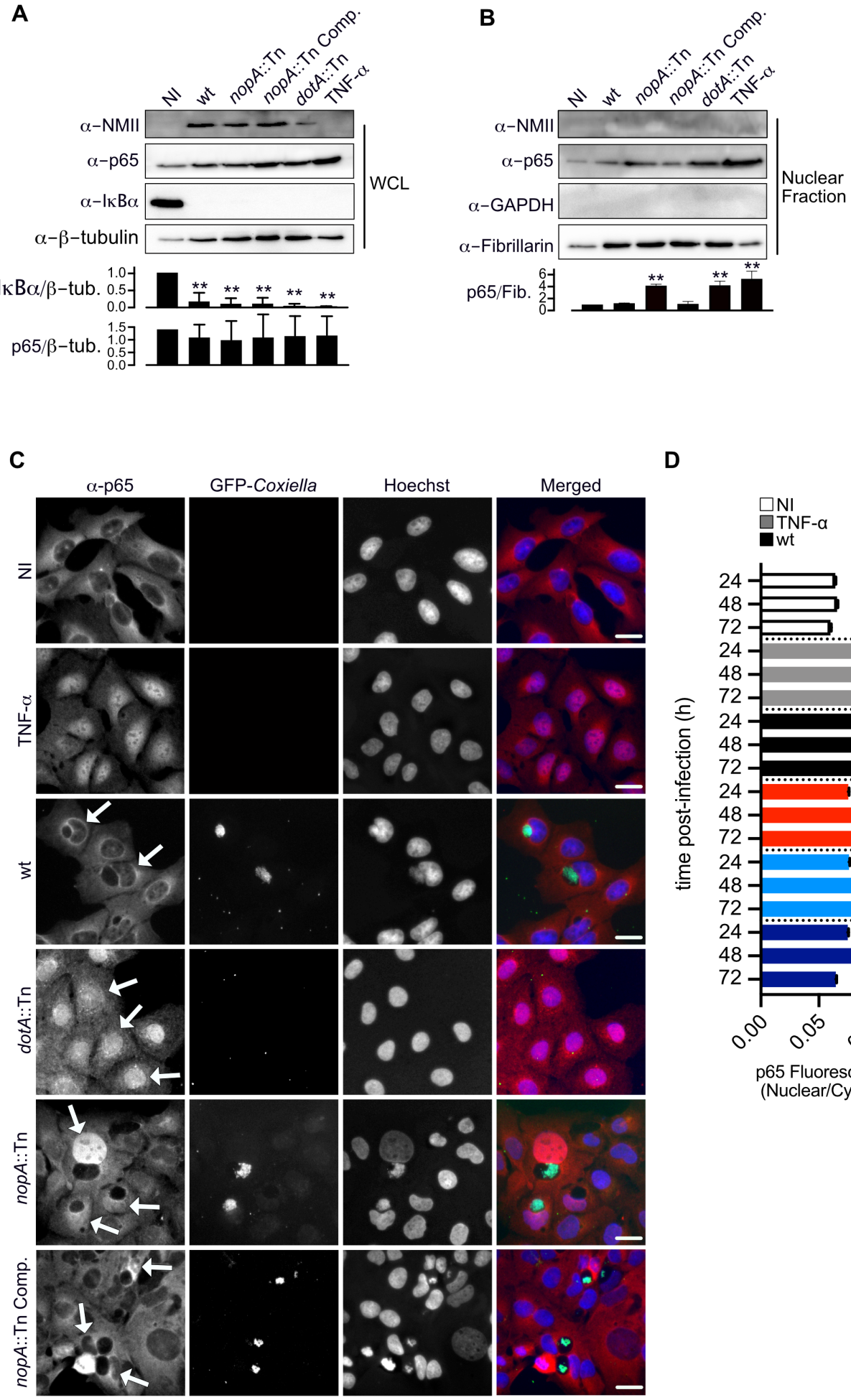
A
NI
wt
nopA::Tn
nopA::Tn Comp.
dotA::Tn
TNF-α
α-NMII
α-p65
α-IκBα
α-β-tubulin
WCL
IκBα/β-tub.
p65/β-tub.
B
α-GAPDH
α-Fibrillarin
Nuclear Fraction
p65/Fib.
C
α-p65
GFP-Coxiella
Hoechst
Merged
D
time post-infection (h)
p65 Fluorescence intensity (Nuclear/Cytoplasm ratio)
n.s.

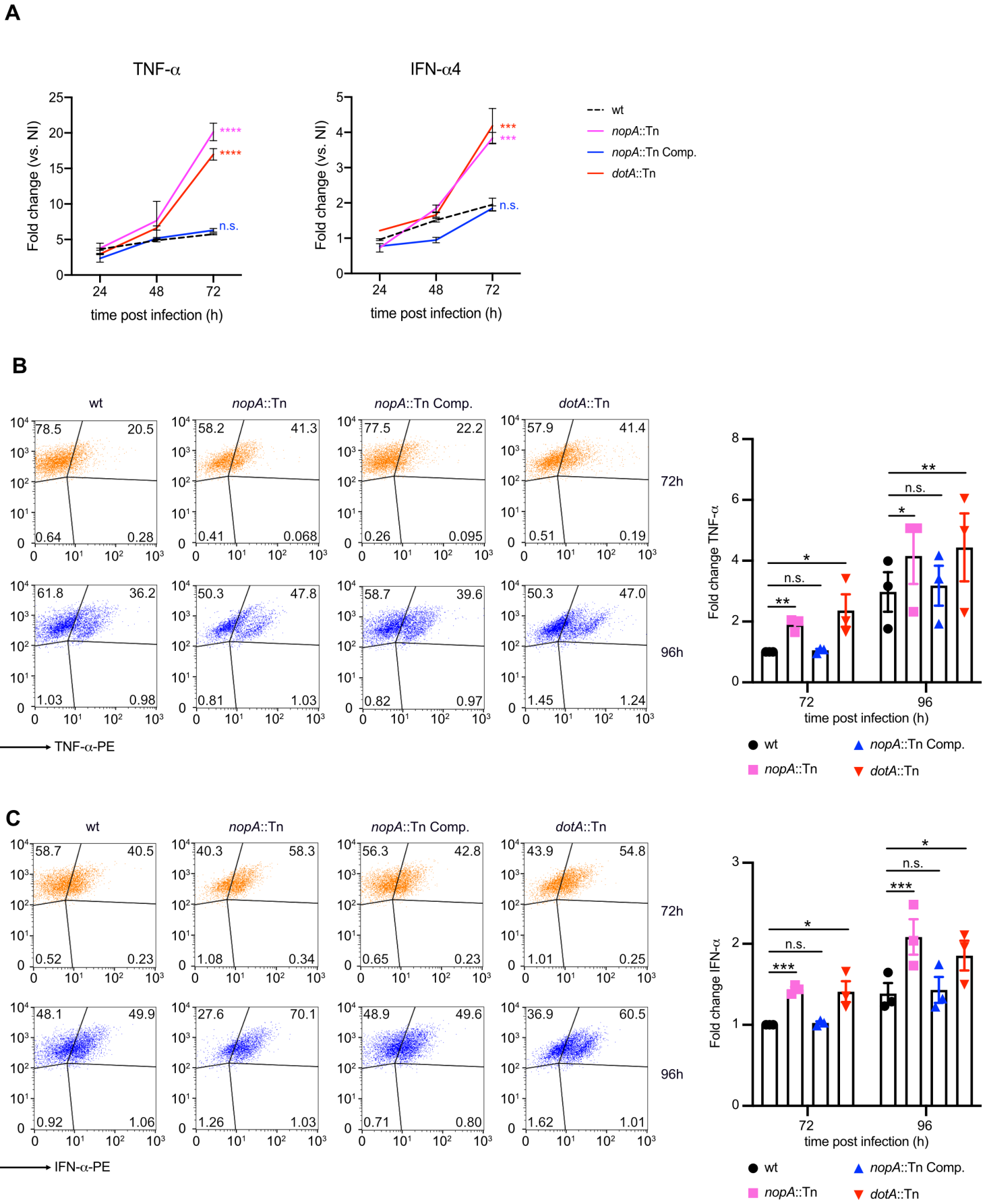
A
TNF-α
IFN-α4
Fold change (vs. NI)
time post infection (h)
wt
nopA::Tn
nopA::Tn Comp.
dotA::Tn
n.s.
B
C
SSC
TNF-α-PE
IFN-α-PE
72h
96h
Fold change TNF-α
Fold change IFN-α